Published online 6 December 2019 *Nucleic Acids Research, 2020, Vol. 48, No. 3* ***1531–1550***
doi: 10.1093/nar/gkz1153

AtFKBP53: a chimeric histone chaperone with functional nucleoplasmin and PPIase domains

Ajit Kumar Singh[1,2], Aritreyee Datta[1], Chacko Jobichen[3], Sheng Luan[4] and Dileep Vasudevan[1,*]

[1]Institute of Life Sciences, Nalco Square, Chandrasekharpur, Bhubaneswar 751023, India, [2]Manipal Academy of Higher Education, Manipal 576104, India, [3]Department of Biological Sciences, 14 Science Drive 4, National University of Singapore, Singapore 117543 and [4]Department of Plant and Microbial Biology, University of California, Berkeley, CA 94720, USA

Received October 23, 2019; Revised November 20, 2019; Editorial Decision November 23, 2019; Accepted December 02, 2019

ABSTRACT

FKBP53 is one of the seven multi-domain FK506-binding proteins present in *Arabidopsis thaliana,* and it is known to get targeted to the nucleus. It has a conserved PPIase domain at the C-terminus and a highly charged N-terminal stretch, which has been reported to bind to histone H3 and perform the function of a histone chaperone. To better understand the molecular details of this PPIase with histone chaperoning activity, we have solved the crystal structures of its terminal domains and functionally characterized them. The C-terminal domain showed strong PPIase activity, no role in histone chaperoning and revealed a monomeric five-beta palm-like fold that wrapped over a helix, typical of an FK506-binding domain. The N-terminal domain had a pentameric nucleoplasmin-fold; making this the first report of a plant nucleoplasmin structure. Further characterization revealed the N-terminal nucleoplasmin domain to interact with H2A/H2B and H3/H4 histone oligomers, individually, as well as simultaneously, suggesting two different binding sites for H2A/H2B and H3/H4. The pentameric domain assists nucleosome assembly and forms a discrete complex with pre-formed nucleosomes; wherein two pentamers bind to a nucleosome.

INTRODUCTION

FK506-binding protein (FKBP) family are ubiquitously found in all life forms, ranging from prokaryotes to higher eukaryotes (1). They are known to catalyze the cis-trans isomerization of prolyl-peptide bonds, thereby accelerating the folding of newly synthesized proteins and possess a conserved five-beta palm-like fold (2–4). The presence or absence of the conserved residues in the PPIase domain essential for FK506-binding and PPIase function segregates the FKBP family members into canonical and non-canonical isoforms (5). Also, based on domain organization, FKBPs are classified as single-domain and multi-domain forms. Single-domain FKBPs are smaller in size and have a single copy of the FK506-binding domain (FKBD), whereas, multidomain FKBPs are larger and have either additional copies of the FKBDs or other functional domain(s) (6). FKBPs are involved in various biochemical processes such as protein folding, protein trafficking, protein assembly, receptor signaling, gene expression, DNA repair and DNA replication (7,8). The PPIase activity of FKBD alone accounts for some of these functions, the rest of which are endowed by the additional domains (9). Among the higher eukaryotes, plants are known to have the largest FKBP family where, *Arabidopsis thaliana* alone encodes for 23 FKBPs (AtFKBPs), consisting of 16 single-domain and 7 multi-domain members (10,11). Out of the 23 AtFKBPs, 2 get targeted to the secretory pathway, 4 to the cytosol, 11 to the chloroplast and 6 to the nucleus (12,13). AtFKBP53, a nuclear targeted multi-domain FKBP, has been reported to have a single FKBD at the C-terminus and an uncharacterized N-terminal domain that functions as a histone chaperone (14). FKBP39 from *Drosophila melanogaster* (DmFKBP39), another multi-domain FKBP, has a conserved pentameric nucleoplasmin fold in its N-terminus and a C-terminal FKBD (15). Similar to AtFKBP53 and DmFKBP39, there are reports of other multi-domain FKBPs performing histone chaperone activity, such as Fpr3 and Fpr4 from *Saccharomyces cerevisiae* and FKBP39 from *Schizosaccharomyces pombe* (SpFKBP39) (16–20). More recently, the presence of a nucleoplasmin-like fold in different FKBPs, including AtFKBP53 has also been suggested (15). The reason for the reported histone chaperone function of AtFKBP53 could perhaps, be attributed to this nucleoplasmin fold.

Nucleoplasmins form a significant class of histone chaperones, defined by a representative N-terminal pentameric

*To whom correspondence should be addressed. Tel: +91 674 2304291; Fax: +91 674 2300728; Email: dileep@ils.res.in

core domain having doughnut architecture with a central pore and an unstructured C-terminal domain. Its oligomerization domain has a unique fold, consisting of eight beta-strands with jelly-roll topology, also described as a beta-sandwich—made up of two opposing four-stranded beta-sheet, giving a triangular or teardrop shape (15,21–26). Nucleoplasmins are widely studied in vertebrates and are broadly classified based on their sequence into four families namely, nucleoplasmin 1 (NPM1), nucleoplasmin 2 (NPM2), nucleoplasmin 3 (NPM3) and nucleoplasmin-like (NPM-like) proteins (27). Members of these nucleoplasmin families are known to interact with the histone H2A/H2B and H3/H4 and exhibit a significant role in controlling the dynamic nature of nucleosomes. In particular, they facilitate the assembly of the basic histone proteins with nucleic acids by restricting the formation of non-specific nucleoprotein complexes and aggregation of histones (28–32). Despite the availability of information regarding the presence of putative NPM isoforms in plants, no studies have focused on their structure or function as histone chaperones. Furthermore, the factors regulating plant chromatin assembly and disassembly processes are not well understood. To understand how nucleosome dynamics is governed in plants by the different histone chaperones, it is essential to conduct detailed structural and functional characterization of these chaperones. We decided to structurally characterize AtFKBP53, the first in the class of nuclear FKBPs in plants, which has been reported to have a putative N-terminal nucleoplasmin core domain and a histone chaperone function. Herein, we report the crystal structure of the C-terminal and the N-terminal domains of AtFKBP53. The C-terminal domain (CTD) possesses the conserved PPIase fold of FKBPs and exists as a monomer, whereas the N-terminal domain (NTD) takes up a very stable pentameric nucleoplasmin fold. We have also confirmed that the nucleoplasmin domain of AtFKBP53 interacts with both histone oligomers and pre-formed nucleosome core particles, as well as plays a role in nucleosome assembly. The highly charged and presumably unstructured middle stretch of the protein might determine the histone affinity and/or specificity, whereas, the C-terminal FKBP domain, though functional as a PPIase, does not seem to have a role in the histone chaperoning activity of AtFKBP53. We firmly believe that the availability of structural information on AtFKBP53 will significantly contribute to improving our understanding of plant chromatin assembly process by this chaperone.

MATERIALS AND METHODS

Preparation of expression constructs

A codon-optimized ORF coding for AtFKBP53 overexpression in *Escherichia coli,* obtained from Genscript (Piscataway, NJ, USA), was used as the template for the preparation of all clones and *E. coli* strain DH5α was used for all cloning procedures. AtFKBP53 NTD (residues 1–100/112) and AtFKBP53 CTD (residues 360–477; FKBD) were cloned in-frame into a pET22b(+) vector between NdeI and XhoI restriction sites for expression with a non-cleavable C-terminal hexa-histidine tag. The AtFKBP53 FKBD was cloned into a pGEX-6P-1 vector between BamHI and XhoI restriction sites for expression with a cleavable N-terminal GST tag, for crystallization experiments.

Protein overexpression and purification

AtFKBP53 domains. The constructs for His-tagged full-length protein and both His-tagged and GST-tagged AtFKBP53 domains were transformed into *E. coli* BL21 (DE3) cells. The transformed cells were grown in 2× YT media containing 100 μg/ml ampicillin, at 37°C to an OD_{600} of 0.5. The overexpression of AtFKBP53 full-length (residues 1–477), NTD (residues 1–100/112) and FKBD (residues 360–477) were induced with 0.2 mM isopropyl β-D-thiogalactopyranoside (IPTG) at 18°C and the overexpression allowed to proceed for 16 hours.

For His-tagged AtFKBP53 and the domains, the cells after overexpression were harvested through centrifugation, resuspended in a buffer containing 50 mM Tris (pH 7.5), 500 mM NaCl, 1 mM β-mercaptoethanol, 10 mM imidazole and 1 mM PMSF and lysed with the help of Vibra-Cell probe-type ultrasonic processor (Sonics). The cell lysate was clarified by centrifugation, and the supernatant was passed through a HisTrap FF 5 ml nickel affinity column pre-equilibrated with the lysis buffer. The bound proteins were eluted using a linear gradient with a buffer containing 20 mM Tris (pH 7.5), 300 mM NaCl, 1 mM β-mercaptoethanol, 1 mM PMSF and 500 mM imidazole. Subsequently, the protein was subjected to size-exclusion chromatography using a HiLoad 16/600 Superdex 200 prep grade column at 4°C in a buffer containing 20 mM Tris (pH 7.5), 150 mM NaCl, 1 mM DTT, 1 mM EDTA and 1 mM PMSF.

For GST-tagged protein, the cells after overexpression and centrifugation were resuspended in a lysis buffer containing 50 mM Tris (pH 7.5), 500 mM NaCl, 1 mM EDTA, 1 mM DTT, 10% glycerol and 1 mM PMSF, and lysed similar to the His-tagged proteins. The cell lysate was clarified by centrifugation, and the supernatant was passed through a GSTrap FF 5 ml column. The GST tag was removed by on-column cleavage of the tag using PreScission protease (GE Healthcare). The cleaved protein was washed out from the column in a buffer containing 20 mM Tris (pH 7.5), 150 mM NaCl, 1 mM EDTA and 1 mM DTT. In order to separate the cleaved protein from small amounts of uncleaved GST fusion protein and GST, the sample was further purified by size-exclusion chromatography using a HiLoad 16/600 Superdex 200 prep grade column at 4°C, in a buffer containing 20 mM Tris (pH 7.5), 150 mM NaCl, 1 mM DTT, 1 mM EDTA and 1 mM PMSF. The purity of peak fractions for both His-tagged and GST-tagged proteins were checked on a 15% SDS-PAGE gel, the pure fractions were subsequently pooled together and concentrated to 22 mg/ml and 15 mg/ml for AtFKBP53 NTD and AtFKBP53 FKBD, respectively.

Core histones. The codon optimized ORFs for the core histones H2A, H2B, H3 and H4 in pET21a(+) vector without any tag were a kind gift from Dr Curt A. Davey (Nanyang Technological University, Singapore). The expression of the core histones followed standard protocols (33,34). In brief, the plasmid constructs were transformed into *E. coli* BL21

(DE3) pLysS cells for the over-expression of individual histones. The cells were grown in 2× YT media at 37°C until the OD_{600} reached 0.6. The over-expression of the individual histones were induced with 0.4 mM IPTG for 3 h at 37°C. The individual histones without any fusion tag were isolated from inclusion bodies and purified under unfolding conditions, following standard protocols (34). The individually purified histone proteins in unfolding condition were dialysed against double-distilled water, aliquoted, lyophilized and stored at −80°C.

Histone refolding and purification

The individually lyophilized core histones were dissolved separately in a denaturing buffer containing 7 M guanidinium hydrochloride. The partner core histones were mixed together in equimolar stoichiometry and dialysed against three changes of a refolding buffer containing 20 mM Tris (pH 7.5), 2 M NaCl, 1 mM EDTA, 10 mM β-mercaptoethanol and 1 mM PMSF to get H2A/H2B dimer, H3/H4 tetramer and histone octamer (33). The obtained histone oligomers were purified in the refolding buffer using a HiLoad 16/600 Superdex 200 prep grade column. The purified histone oligomers were stored in 50% glycerol at −20°C.

Preparation of '601' DNA

Eight copies of strong-positioning '601' DNA (145 bp), cloned into pUC57 vector with EcoRV restriction sites in between was a generous gift from Dr Curt A. Davey (Nanyang Technological University, Singapore). The plasmid was amplified by transformation to *E. coli* HB101 cells that were grown for about 20 h. The plasmid was isolated by the alkaline lysis method, followed by phenol-chloroform extraction to remove RNA and contaminating proteins. The 145 bp insert was cut out from the plasmid by restriction digestion using EcoRV. The 145 bp insert DNA was then separated from the cut plasmid by a PEG fractionation step (35).

Nucleosome core particle reconstitution

Purified histone octamer and 145 bp '601' DNA were mixed in equimolar stoichiometry in a 2.0 M KCl (high salt) buffer condition and was dialysed down in slow steps to low salt buffers and finally brought into a buffer without salt (33,35). As salt concentration got reduced gradually, the DNA strand got associated with histone octamer to form nucleosome core particles (NCP). The reconstituted NCP was further checked on a native 6% DNA–PAGE gel.

Circular dichroism spectroscopy

Circular dichroism (CD) spectra were measured on a Chirascan circular dichroism spectrometer (Applied Photophysics) using a quartz cuvette with a path length of 2.0 mm. Protein sample (AtFKBP53 NTD) at a concentration of 0.05 mg/ml in 50 mM phosphate buffer was used to obtain the spectra in the far-ultraviolet (UV) region (190–260 nm). The obtained spectrum was deconvoluted using Dichroweb software (36) to calculate the percentage of secondary structural elements present in the protein.

Pull-down assays

To check for the interaction of AtFKBP53 NTD with histones, 5 μM of His-tagged AtFKBP53 NTD (1–112)/FKBD (360–477) was mixed with 20 μM of reconstituted H2A/H2B or H3/H4. The samples were then incubated with Talon metal affinity resin beads (Clontech) pre-equilibrated with a buffer containing 20 mM Tris (pH 7.5), 300 mM NaCl, 30mM imidazole (pH 7.5), 10μg/ml BSA and 1.0 mM β-mercaptoethanol for 30 min at 4°C. The resin beads were then washed with thirty column volumes of wash buffer containing 20 mM Tris (pH 7.5), 300 mM NaCl, 50 mM imidazole (pH7.5), 0.2% Tween-20 and 1.0 mM β-mercaptoethanol. The resin-bound complexes were eluted with a buffer containing 20 mM Tris (pH 7.5), 300 mM NaCl, 500 mM imidazole (pH7.5) and 1 mM β-mercaptoethanol, and analysed on 18% SDS-PAGE, after staining with Coomassie Brilliant Blue R 250 (37,38).

Pull-down assay was also used to check whether H2A/H2B can replace H3/H4 bound to AtFKBP53 NTD. Towards this end, H2A/H2B was passed in increasing concentrations of 20–60 μM through the Talon resin beads having AtFKBP53 NTD–H3/H4 complex, after the washing step. Similarly, to check whether H3/H4 can replace H2A/H2B bound to AtFKBP53 NTD, H3/H4 was passed in increasing concentrations of 20–60 μM through the beads having AtFKBP53 NTD–H2A/H2B complex, after the washing step. The resin-bound complexes were eluted and analysed, as mentioned earlier.

Pull-down assay was used to study the salt stability of AtFKBP53 NTD complexes with H2A/H2B and H3/H4 as well. Herein, the complexes were incubated with buffers having NaCl concentrations varying from 0.3 M to 1 M, in separate reactions, the resin beads with bound complexes were washed with the same buffer, and the resin-bound proteins were eluted and analysed together on 18% SDS-PAGE.

Analytical size-exclusion chromatography

To study the oligomeric status of AtFKBP53 NTD (residues 1–100/112) and AtFKBP53 FKBD (residues 360–477), 0.5 mg/ml solutions of either of the proteins in a buffer containing 20 mM Tris (pH 7.5), 150 mM/300 mM NaCl, 1 mM β-mercaptoethanol were subjected to analytical size-exclusion chromatography using a Superdex 200 10/300 GL column connected to an AKTA Pure 25M machine maintained at 4°C.

To study the interaction of AtFKBP53 NTD with the individual histone oligomers such as H2A/H2B and H3/H4, 5 μM of purified AtFKBP53 NTD (residues 1–112) was mixed with 10 μM of refolded H2A/H2B and H3/H4 separately in a buffer containing 20 mM Tris (pH 7.5), 300 mM NaCl, 1 mM β-mercaptoethanol. The mixed samples were then incubated for 30 min at 4°C and subjected to analytical size-exclusion chromatography as mentioned above for the individual domains. Eluted protein was analysed on 18% SDS-PAGE after staining with Coomassie Brilliant Blue R 250.

For co-interaction studies of AtFKBP53 NTD with the histone oligomers H2A/H2B and H3/H4, 5 μM of purified AtFKBP53 NTD (residues 1–112) was mixed with 10

μM each of refolded H2A/H2B and H3/H4 in a buffer containing 20 mM Tris (pH 7.5), 300 mM NaCl, 1 mM β-mercaptoethanol. The mixed samples were then incubated for 30 min at 4°C and subjected to analytical size-exclusion chromatography. Eluted protein was analysed on 18% SDS-PAGE after staining with Coomassie Brilliant Blue R 250.

Similarly, to study binding of AtFKBP53 NTD with AtFKBP53 FKBD, 37 μM of purified AtFKBP53 NTD (residues 1–112) was mixed with 37 μM of purified AtFKBP53 FKBD (residues 360–477) in a buffer containing 20 mM Tris (pH 7.5), 150 mM NaCl, 1 mM β-mercaptoethanol and 1 mM PMSF, incubated on ice for 30 minutes and subjected to analytical size-exclusion chromatography and analysed as mentioned above.

To study the thermal stability of AtFKBP53 NTD pentamer, the protein sample was subjected to different temperatures and then individually passed through a Superdex 200 10/300 GL column, equilibrated with a buffer containing 20 mM Tris (pH 7.5), 300 mM NaCl and 1 mM β-mercaptoethanol at 4°C. Salt stability of the pentamer was checked by performing analytical size-exclusion chromatography of the protein sample at 4°C, using the same column, in buffers containing varying concentrations of NaCl (ranging from 150 mM to 2 M). Analytical size-exclusion chromatography was used to check the stability of the protein to increasing concentrations of urea by incubating the protein samples in buffers containing the respective urea concentration for 16 hours at room temperature and then passing through a Superdex 75 10/300 GL column, equilibrated with a buffer having the same urea concentration, also at room temperature.

Electrophoretic mobility shift assay

To study the binding of AtFKBP53 NTD and AtFKBP53 FKBD with NCP, purified AtFKBP53 NTD/FKBD/BSA and NCP were mixed, in a buffer containing 20 mM Tris (pH 7.5), 50 mM NaCl, 1.0 mM EDTA and 1.0 mM DTT. The mixtures were incubated at 4°C for 1 hour and subjected to electrophoresis on a 6% Native PAGE in 0.5× TBE buffer for 180 min at 60 V and stained with ethidium bromide (EtBr) for visualization.

Chymotrypsin-coupled Peptidyl-prolyl cis/trans isomerase assay

Peptidyl-prolyl cis/trans isomerase (PPIase) activity was analysed using a protease-coupled assay (39) in a Varian Cary 300 Bio UV–visible double-beam spectrophotometer equipped with a Peltier system to maintain temperature. In the PPIase assay we used, a functional PPIase domain is expected to convert the *cis* conformation of the prolyl-bond in a peptide having a proline residue and a C-terminal *p*-nitroanilide (pNA) moiety, into *trans* conformation, which in turn favors the cleavage of the chromogenic pNA moiety by the α-chymotrypsin enzyme. The subsequent release of *p*-nitroaniline could be measured at 390 nm in a time-resolved manner, which served as an indicator of the enzymatic activity (40). 250 μM of the substrate peptide *N*-succinyl-ala-ala-pro-phe-*p*-nitroanilidine in lithium chloride/tetrahydrofuran solution, 60 mg/ml of α-chymotrypsin in 2.0 mM of calcium chloride (pH 7.5) and 781.25 μM AtFKBP53 FKBD in a buffer containing 20 mM Tris (pH 7.5) and 150 mM NaCl were the stock solutions used for the experiment. 30 μM of the substrate peptide was mixed with 210 μg of α-chymotrypsin and three different amounts (60, 65 and 90 μg) of AtFKBP53 FKBD. The volume was made up to 1 ml using the buffer containing 20 mM Tris (pH 7.5) and 150 mM NaCl. The uncatalyzed reaction was performed in the absence of AtFKBP53 FKBD, while 400 μg BSA was used as a negative control. The assay was performed at 10°C for a time period of 300 s. The spectrum of the hydrolysed peptide was recorded at 390 nm using a quartz cuvette having a path length of 1 cm. It may be noted that AtFKBP53 FKBD remained intact in the presence of α-chymotrypsin used for cleavage of the substrate, for up to 300 s, the maximum time till which the time-resolved assay was performed (Supplementary Figure S2C).

Analytical ultracentrifugation

To study the binding of AtFKBP53 NTD with NCP and histone oligomers, sedimentation velocity analytical ultracentrifugation (AUC) experiment was performed using a ProteomeLab XL-1 analytical ultracentrifuge (Beckman Coulter). Epon double-sector centrepieces were filled with 400 μl of the sample buffer and 375 μl of AtFKBP53 NTD and histone/NCP complexes having an OD_{280} of 0.4–0.8, respectively in the two sectors. The samples were centrifuged at 40 000 rpm for histones and 30 000 for NCP complexes, at 20°C. Frames were collected until sedimentation was complete. Absorbance data at 280 nm was acquired by taking two averages per scan. Absorbance scans were taken at an interval of 3 minutes. Sample buffer density, viscosity and partial specific volume of protein complexes were calculated by the software SEDNTERP (41), data analysis was performed by SEDFIT program using c(S) distribution analysis, and figures were prepared using GUSSI (42).

Small-angle X-ray scattering

Small-angle X-ray scattering (SAXS) data for AtFKBP53 NTD were collected at the BioSAXS beamline BM29 in Grenoble (France). Protein samples with a concentration of 1.5 mg/ml in a buffer containing 20 mM Tris (pH 7.5) and 300 mM NaCl were used for the experiment. 300 mM NaCl-containing buffer alone was used to avoid non-homogeneity of the sample due to the presence of mixed oligomeric states. Samples were loaded into the measurement cell and exposed to X-rays. Scattering data was collected using the robotic sample handling available at the beamline, at a temperature of 10°C using a camera length of 2.8 m covering a range of momentum transfer $0.04 \leq Q \leq 4.9$ nm^{-1} ($Q = 4\pi\sin\theta/\lambda$, where 2θ is the scattering angle and $\lambda = 0.998$ Å is the X-ray wavelength). Ten frames were recorded, and all the frames were averaged and subtracted with the buffer using PRIMUS (43). The data processing was carried out with ATSAS program (43) to obtain the radius of gyration (R_g), Maximum particle dimension (Dmax), excluded particle volume (V_p) and the pair distribution function ($P(r)$). *Ab initio* low-resolution molecular envelope in P1 symmetry (globular shape) and P5 symmetry (star shape) were generated using DAMMIF (44). The P5 symmetry model was

generated based on the fact that all structurally characterized nucleoplasmin family members exist as a pentamer. The 20 independent models generated by DAMMIF (44) were averaged using DAMAVER (45) to generate a low-resolution model. (NSD value in Supplementary Table S3) CRYSOL (46) was used to compare the calculated scattering curves from the crystal structure and the low-resolution model of AtFKBP53 NTD, with experimental scattering curves. The generated *ab initio* model, along with its crystal structure overlapped model, were rendered using PyMOL (Schrödinger, LLC).

Isothermal titration calorimetry

AtFKBP53 NTD, H2A/H2B and H3/H4 were dialyzed in a buffer containing 20 mM PIPES (pH 7.4), 300 mM NaCl and 1 mM β-mercaptoethanol. Whereas, for NCP interaction studies, AtFKBP53 NTD and NCP were dialysed in 20 mM Tris (pH 7.5), 50 mM NaCl and 1 mM β-mercaptoethanol overnight at 4°C. Isothermal titration calorimetry (ITC) experiments were carried out using MicroCal PEAQ-ITC (Malvern Instruments) at 25°C. Here, 10–15 μM of histone oligomers/ 6–8 μM of NCP were loaded in the reaction cell, and 120–150 μM of AtFKBP53 NTD was taken in the syringe. The heat of dilution generated for the AtFKBP53 NTD when titrated into the buffer was used to correct the data. The binding isotherms were fitted to a 'one-site' binding model for histone interaction and 'sequential' binding model for NCP interaction using MicroCal PEAQ-ITC analysis software. The experimental data shown is an average of three independent experiments.

Histone chaperone assay

Histone chaperone assay by plasmid supercoiling was performed as has been described before (47,48). The negatively supercoiled pUC19 plasmid (500 ng) was pre-incubated with 0.5 U of Wheat Germ Topoisomerase 1 (Inspiralis) in a reaction volume of 50 μl at 37°C for 40 min. In a separate 50 μl reaction, a mixture of 2 μM H2A/H2B and 2 μM H3/H4 along with increasing concentrations of AtFKBP53 NTD (1–3 μM) were incubated in an assembly buffer containing 20 mM Tris (pH 7.5), 100 mM NaCl, 1 mM $MgCl_2$, 0.5 mM DTT and 0.1 mg/ml BSA at 30°C for 30 min. Later, the AtFKBP53 NTD-H2A/H2B-H3/H4 mix and the pretreated plasmid were mixed together and incubated further at 37°C for 90 min. The reaction was stopped by adding an equal volume of a stop buffer containing 20 mM EDTA, 1% (w/v) SDS, 0.2 mg/ml proteinase K and incubating at 37°C for 30 min. After the reaction completion, plasmids were extracted using phenol-chloroform treatment and resolved on 1% agarose gel followed by ethidium bromide staining.

Crystallization, data collection and data processing

A sample of 15 mg/ml concentration of AtFKBP53 FKBD (in complex with FK506 compound) and another of 22 mg/ml concentration of AtFKBP53 NTD (residues 1–100) were subjected to crystallization screening using different commercial screening kits. Crystals of AtFKBP53 FKBD and AtFKBP53 NTD appeared in sitting-drop vapor diffusion plates in several conditions which were further optimized. A rhomboid crystal of AtFKBP53 FKBD from a condition having 0.1 M Tris (pH 8.5), 3 M NaCl and a single rod-shaped crystal of AtFKBP53 NTD from an optimized condition having 0.2 M DL-Malic acid (pH 7.0), 25% (w/v) Polyethylene glycol 3350 were used for data collection. The AtFKBP53 NTD crystal obtained from the above condition was transferred into a cryoprotectant solution containing the reservoir solution supplemented with 20% glycerol and then flash cooled in liquid nitrogen; whereas, the AtFKBP53 FKBD crystal was directly flash cooled in liquid nitrogen without the use of any cryoprotectant.

A high-resolution dataset for AtFKBP53 FKBD was collected at the beamline BL21 of RRCAT (Indore, India) and recorded with a MarCCD detector. The diffraction data were processed using iMOSFLM (49). The crystal belonged to the primitive orthorhombic space group $P2_12_12_1$ with unit cell dimensions $a = 42.9$ Å, $b = 48.0$ Å, $c = 59.30$ Å, $\alpha = \beta = \gamma = 90°$. The preliminary diffraction data collection for AtFKBP53 NTD was carried out at the X-ray diffraction facility of Indian Institute of Chemical Technology (IICT; Hyderabad, India) on an R-axis IV++ machine equipped with an image plate detector. A high-resolution dataset was later collected at the beamline BM14 of ESRF (Grenoble, France) and recorded with a MarCCD detector. The diffraction data were processed using iMOSFLM. The crystal belonged to the primitive monoclinic space group $P2_1$ with unit cell dimensions $a = 56.59$ Å, $b = 97.39$ Å, $c = 96.43$ Å, $\alpha = \gamma = 90°$ and $\beta = 94.12°$. Both the datasets were further processed by AIMLESS (50) from the CCP4 suite (51).

Structure determination

The crystal structure of AtFKBP53 FKBD (residues 360–477) was solved by molecular replacement method with the help of program MolRep (52) from CCP4 suite, using the coordinates of the A54E mutant of *Burkholderia pseudomallei* FKBP-FK506 complex structure as a search model (PDB ID: 3UQA), but without FK506. One molecule was present in one asymmetric unit. Model building and structure refinement were carried out using COOT (53) and Refmac5 (54) from the CCP4 suite. The structures were analysed for stereochemical quality using the program MolProbity (55). The structure figures and structural superpositions were prepared and calculated using the PyMOL molecular graphics system.

The crystal structure of AtFKBP53 NTD (1-100) was solved by molecular replacement method with the help of program Phaser-MR (56) in Phenix (57), using the coordinates of *X. laevis* nucleoplasmin monomer structure as a search model (PDB ID: 1K5J). Ten molecules were present in one asymmetric unit. Model building, structure refinement, analysis of stereochemical quality, structural superpositions and preparation of structure figures were carried out as described above. Both the structures have been deposited to PDB with the accession IDs 6J2M and 6J2Z.

RESULTS

Structure of AtFKBP53 FKBD reveals a canonical fold

AtFKBP53 has a putative FK506-binding domain (FKBD) between residues 360 and 477, at its C-terminus (hereafter referred to as AtFKBP53 FKBD) resulting in its classification as an FKBP (58). AtFKBP53 FKBD showed ∼50% sequence identity with the structurally characterized HsFKBP12, HsFKBP13 and BpFKBP, indicating that it might possess a similar structural fold (Figure 1A). To characterize the putative FKBD in AtFKBP53 structurally, we solved its crystal structure at 1.13 Å resolution, in complex with FK506, one of the well-known interacting partners of the FKBP family of proteins (6). Our attempts to crystallize the FKBD in the absence of FK506 were not successful. The data collection and refinement statistics are provided in Table 1. The complex was crystallized in the $P2_12_12_1$ space group, where one molecule of the FKBD-FK506 complex was present in an asymmetric unit. The structure was solved using the molecular replacement method, using the coordinates of an A54E mutant of *Burkholderia pseudomallei* FKBD-FK506 structure (PDB ID: 3UQA) as the search model, but without FK506. Crystal structure of the complex showed that AtFKBP53 FKBD has the characteristic, conserved five-beta palm-like fold, wrapping over helical segments (Figure 1B, C; Supplementary Figure S1A), like other structurally characterized FKBDs. The five-beta framework includes β1 (371–377), β2 (391–400), β3a (406–409), β3b (416–419), β4 (441–445), and β5 (467–475): whereas the short α-helical segments comprise of residues spanning 427–434 and 448–450. The FK506 compound binding pocket in the concave face of the palm-like fold (Figure 1D) is lined with eleven conserved residues (Figure 1E). Three of the conserved residues are involved in hydrogen bond formation with FK506: Ile^{426}-NH to C-1 lactone carbonyl, Asp^{408}-CO_2^- to C-10 hemiketal hydroxyl and Tyr^{452}-OH to C-8 amide oxygen (Figure 1D, Supplementary Figure S1B and Supplementary Table S1) whereas, the six conserved aromatic residues (Tyr^{396}, Phe^{416}, Phe^{469}, Val^{425}, Ile^{426} and Trp^{429}) form a hydrophobic hub that further strengthens the binding of the FK506 compound (Figure 1E). Ramachandran plot values revealed no outliers.

The calculated RMSD value (0.74) obtained from the superimposition of the main chains of AtFKBP53 FKBD and the well-characterized HsFKBP12 (PDB ID: 1FKJ) (Supplementary Figure S1C) indicates the overall fold of the two proteins to be identical, with only minor variations in the lengths and the trajectories of the β-strands. We also carried out the pairwise superimposition of the binding pocket for both the proteins, revealing a similar orientation of the eleven conserved residues and their interaction pattern with FK506 (Figure 1E). Put together; the above results suggest that AtFKBP53 FKBD is a canonical PPIase.

AtFKBP53 FKBD is a monomer in solution with PPIase activity

Having confirmed AtFKBP53 FKBD to have the characteristic PPIase fold, we then investigated the oligomeric status and PPIase activity of AtFKBP53 FKBD in solution. The analytical size-exclusion chromatography (analytical SEC) profile confirmed the monomeric nature of the domain having an apparent molecular mass of 12.8 kDa, in accordance with that of other reported FKBDs (51) (Supplementary Figure S2A). The previous study has not indicated whether AtFKBP53 is an active PPIase (14). It is also possible that as a multi-domain FKBP, AtFKBP53 might have gained additional functions by virtue of other functional domains and in the process might have become inactive as a PPIase. It concerned us to verify if AtFKBP53 FKBD is indeed a PPIase. Amino acid sequence analysis revealed the presence of all the eleven residues responsible for PPIase activity (and FK506-binding) in its FKBD (59) (Figure 1A). A standard enzymatic PPIase assay was used to study its activity, as previously described (40). Addition of increasing amounts of AtFKBP53 FKBD to a peptide substrate containing a *cis*-prolyl bond conjugated to a *p*-nitroanilide moiety, showed a steady, time-dependent increase in the intensity of the absorption maxima of p-nitroaniline indicating that it was functional as a PPIase (Supplementary Figure S2B). The uncatalyzed reaction and the negative control also had some basal absorbance at 390 nm, attributable to the unstable *cis* conformation of the peptide, which allowed some amount to readily convert to its *trans* conformation under the reaction conditions (Supplementary Figure S2B).

Sequence, phylogenetic and secondary structural analyses suggest AtFKBP53 to be a nucleoplasmin

AtFKBP53 has been reported to be a member of the newly identified FKBP nucleoplasmins, possessing an N-terminal nucleoplasmin domain and a C-terminal FKBD (15). A sequence alignment of AtFKBP53 NTD (residues 1–96) with other structurally characterized nucleoplasmins such as DmFKBP39-NLP, XlNPM, HsNPM1, HsNPM2, XlNO38-NPM, MmNPM1 and DmNLP (Supplementary Figure S3A) showed <22% sequence identity between them, while the phylogenetic analysis showed DmFKBP39-NLP to be the closest relative to AtFKBP53 NTD (Supplementary Figure S3B). The low degree of sequence conservation could not allow AtFKBP53 NTD to get classified as nucleoplasmin with confidence. Subsequently, deconvolution of CD spectra of AtFKBP53 NTD showed it to be predominantly composed of β-strands (49%) (Supplementary Figure S4A). This hinted towards AtFKBP53 NTD taking up a β-rich nucleoplasmin-fold based on the previous studies that have shown nucleoplasmin to be a pentamer, wherein each monomer possesses a β-sandwich topology (15,21–26).

Crystal structure analyses confirm AtFKBP53 NTD to be a nucleoplasmin

A crystal obtained for AtFKBP53 NTD diffracted to 2.4 Å resolution and belonged to $P2_1$ space group. A total of ten molecules were expected to be present in an asymmetric unit, based on the Matthews Coefficient calculations. The structure was solved by molecular replacement, using the coordinates of a monomer from *X. laevis* nucleoplasmin core pentamer structure (PDB ID: 1K5J) as a model and searching for ten molecules in the asymmetric unit. It may be noted that *X. laevis* nucleoplasmin core domain

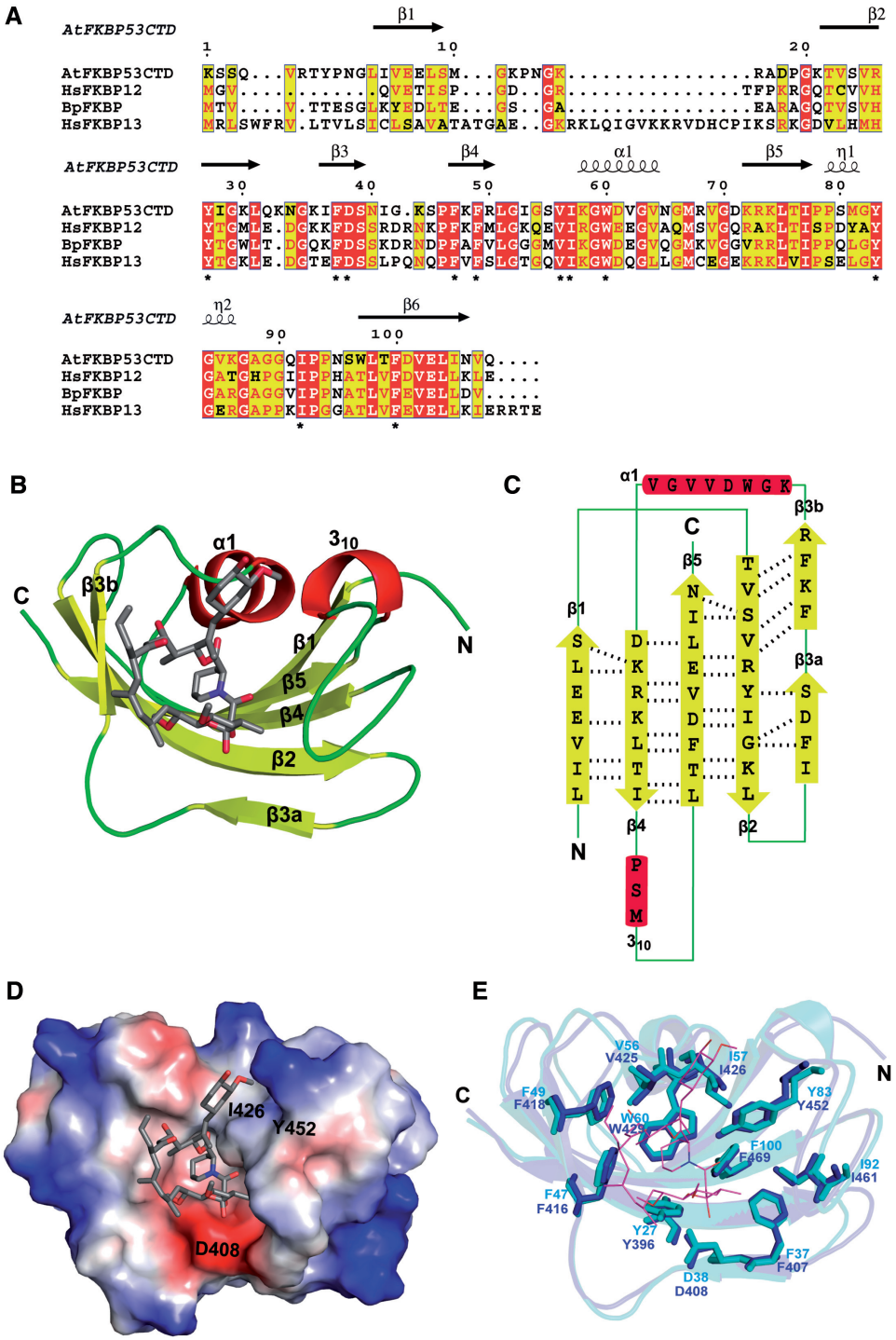

Figure 1. Sequence alignment and crystal structure of AtFKBP53 CTD reveals a canonical FKBD fold. (**A**) Multiple sequence alignment of AtFKBP53 FKBD with human FKBP12 (HsFKBP12; UniProtKB – P62942), human FKBP13 (HsFKBP13; UniProtKB – P26885) and *Burkholderia pseudomallei* FKBP (BpFKBP; UniProtKB – Q63J95) was done using the T-Coffee program. The indicated residue numbering is based on hFKBP12, and secondary structures are based on AtFKBP53 CTD. The red coloured box highlights strictly conserved residues and the yellow coloured box highlights residues that are semi-conserved. The strictly conserved eleven residues known to play a role in PPIase activity and FK506-binding are marked by *. (**B**) Cartoon representation of AtFKBP53 FKBD in complex with FK506, showing the α-helices (red), β-strands (yellow), and loops (green). FK506 compound is shown as a stick model with elements highlighted in different colours (grey, C; blue, N; and red, O). (**C**) 2D topology diagram of AtFKBP53 FKBD with β-strands shown as arrows (yellow), α-helices as boxes (red), loops as lines (green) and the hydrogen bonding patterns between β-strands marked with dotted lines. (**D**) Electrostatic surface charge distribution of AtFKBP53 FKBD with a linear colour ramp of red (–kT) to blue (+kT) where the residues in the binding pocket involved in direct hydrogen bonding with FK506 are highlighted. FK506 compound is shown as a stick model with the elements highlighted in different colours (grey, C; blue, N; and red, O). (**E**) Superposition of crystal structure of AtFKBP53 FKBD (blue) with FKBP12 from *H. sapiens* (cyan) (HsFKBP12; PDB ID: 1FKJ); the 11 conserved residues involved in FK506-binding are represented as sticks and FK506 compound from 1FKJ as lines with elements highlighted in different colours (magenta, C; blue, N; and red, O).

Table 1. Data collection, processing and refinement statistics

Parameter	AtFKBP53 FKBD	AtFKBP53 NTD
Data collection & processing		
Beamline	RRCAT-BL21, Indore, India	ESRF-BM14, Grenoble, France
Detector type	Marmosaic CCD	Marmosaic CCD
Wavelength (Å)	0.9794	0.9537
Data collection temperature (K)	103	100
Space group	$P2_12_12_1$	$P2_1$
a, *b*, *c* (Å)	43.04, 48.19, 59.50	56.59, 97.39, 96.43
α, β, γ (°)	90.00, 90.00, 90.00	90.00, 94.12, 90.00
Resolution (Å)	28.25–1.13 (1.13–1.15)	68.53–2.40 (2.49–2.40)
R_{merge} (%)	6.4 (29.0)	6.3 (50.9)
$I/\sigma I$	15.4 (5.0)	16.5 (3.2)
CC (1/2) (%)	0.998 (0.957)	99.9 (90.5)
No. of unique reflections	46611 (2254)	40837 (4267)
Mosaicity	0.38	0.71
Completeness (%)	99.3 (98.5)	100.0 (100.0)
Multiplicity	7.2 (6.8)	6.6 (6.5)
Wilson *B*-factor (Å^2)	6.36	56.5
Matthew's coefficient (Å^3/Da)	2.42	2.38
Solvent content (%)	49.19	43.79
No. of molecules in ASU	1	10
Refinement		
No. of unique reflections	44215	38867
R_{work}/R_{free} (%)	12.6/14.5	20.4/23.3
Total no. of non-H atoms	1000	7210
No. of water molecules	92	38
No. of ligands	1 FK506; 14 Cl	0
Mean *B*-factor (Å^2)	12.69	69.0
RMSDs:		
Bond lengths (Å)	0.020	0.009
Bond angles (°)	2.088	1.527
Ramachandran plot values (%):		
Favoured/outliers	100/0	97.5/2.5

shares only 17.3% sequence identity with AtFKBP53 NTD. It is the identification of AtFKPB53 NTD as a nucleoplasmin based on domain, sequence and secondary structure analyses that allowed us to use a molecular replacement model with such low sequence identity with the template. Table 1 provides data collection and refinement statistics. The solved and refined structure revealed two independent pentamers, but the two pentamers did not stack on top of each other to form a decamer.

One of the pentamers that had better electron density was used for the detailed structural analyses and figure preparations. The discrete pentameric structure made up of five monomers (Figure 2A) had the N and C -termini of each monomer going in and coming out from the same proximal face (Figure 2B, C). A monomer is characterized by an eight-stranded beta-fold with a jelly roll topology, also described as a beta-sandwich fold (Figure 2B, C). This topology is a signature fold of nucleoplasmin family members, confirming AtFKBP53 NTD to be typical nucleoplasmin. The 5-fold axis of the pentamer runs parallel to the individual beta strands (Figure 2B). Among the strands, β6 is the closest to the 5-fold axis, whereas the β-hairpin consisting of β4 and β5 gets twisted out and stays farthest from the axis. The jelly roll topology of AtFKBP53 NTD gets stabilized by regular hydrogen bonding between the antiparallel beta-strands, with the pattern being disturbed at certain places by beta bulges which generate a kink on strands β3 and β5, and a break in β6 (Figure 2B, C). An aromatic corner made up of the four amino acids Phe3, Trp4, Phe93 and Tyr96 is present in each monomer and faces towards the inner side of the barrel (Figure 2B). The analysis of the structure revealed 2.5% residues to be Ramachandran outliers. A closer examination revealed that most of these outliers are glycine, pre-proline or proline residues.

The crystal structures of AtFKBP53 NTD and *X. laevis* nucleoplasmin core domain (XlNPM; PDB ID: 1K5J), the first structurally characterized nucleoplasmin were compared (Supplementary Figure S4B). Both the structures have the typical eight-beta organization of nucleoplasmins. However, the structure of AtFKBP53 NTD has some differences as compared to that of XlNPM. A 3_{10} helix is present in AtFKBP53 NTD between the strands β2 and β3, unlike that of *X. laevis* nucleoplasmin, where the corresponding stretch is disordered and forms the acidic stretch A1 (EDDEE). In contrast, the well-resolved acidic stretch A1 (DDDDE) in the AtFKBP53 NTD crystal structure is present between the beta-strands β6 and β7; albeit on the same face as that of XlNPM (Supplementary Figure S4B). The A1 tract is thought to contribute considerably to the histone-binding characteristic of nucleoplasmins. The conserved 'GSGP' motif present between the strands β7 and β8 of XlNPM is absent in AtFKBP53 NTD and has a 'GDRS' motif instead (Supplementary Figure S4B), similar to the 'GDAS' motif of DmFKBP39 nucleoplasmin-like domain. The β-hairpin motif of XlNPM is longer and stretches out of the beta-sandwich structure, whereas the same motif in AtFKBP53 NTD stays closer to the beta-sandwich structure and has a longer loop between β4 and β5.

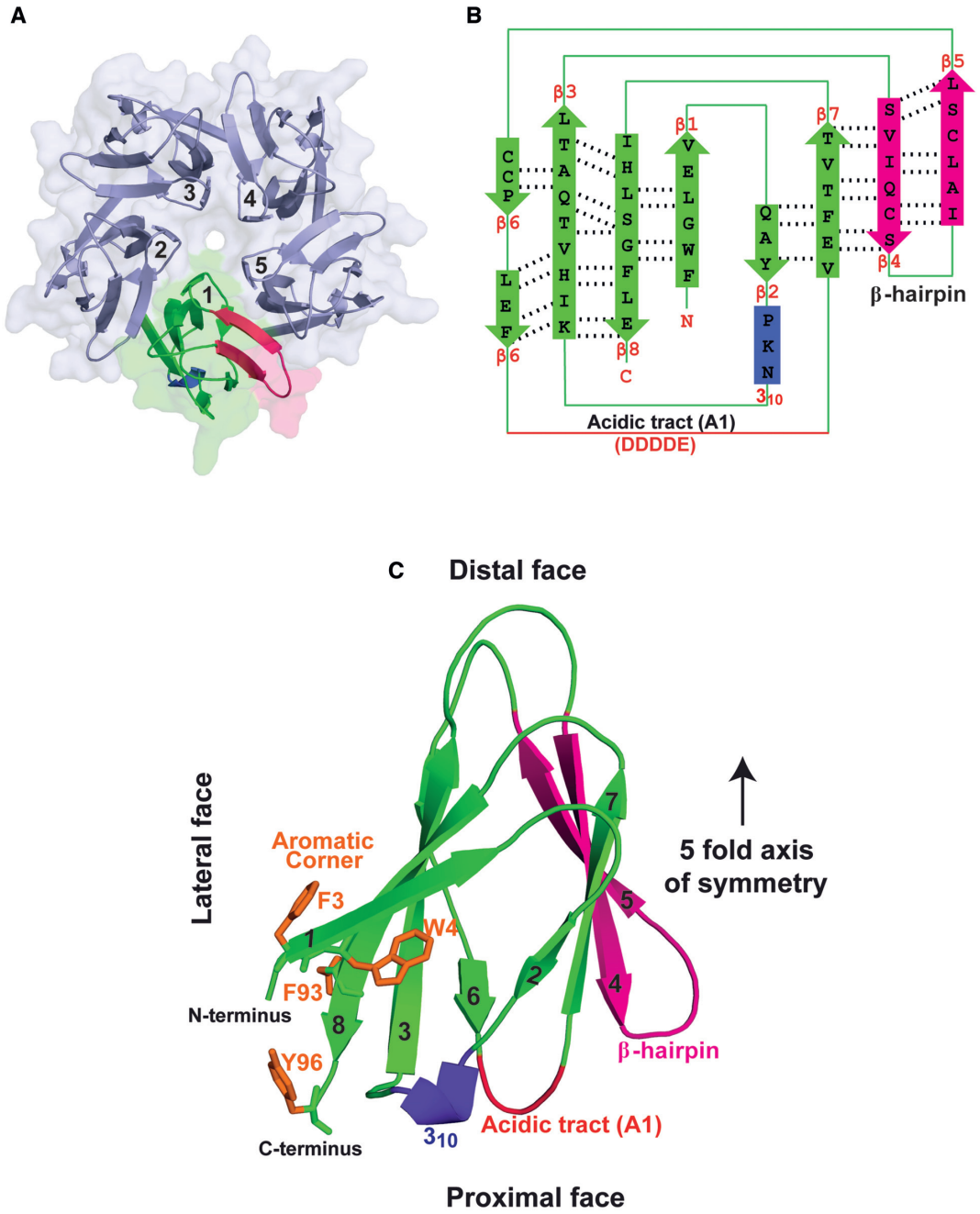

Figure 2. Crystal structure of AtFKBP53 NTD reveals a nucleoplasmin fold. (**A**) Cartoon and surface representation of the crystal structure of AtFKBP53 NTD pentamer, wherein one monomer is highlighted in different colours. (**B**) 2D jelly-roll topology diagram of the monomer, showing the arrangement of the β strands, with the hydrogen bonding patterns marked with dotted lines. The acidic tract A1 formed of residues DDDDE, the 3_{10} helix, and the β-hairpin motif are also labelled. (**C**) Cartoon representation of AtFKBP53 NTD monomer having the characteristic teardrop shape, labelled for the distal, lateral and proximal faces and the five-fold axis of symmetry (with a black arrow). The N and the C-terminal ends go in and come out respectively, from the proximal face. The aromatic corner made up of F3, W4, F93, Y96 (stick representation, with side-chains in orange), the 3_{10} helix (in purple), and the β-hairpin motif formed by β4 and β5 (in pink) are also highlighted.

To understand the structural similarities of AtFKBP53 NTD with other known nucleoplasmin structures, we did a PDB eFold search with the monomer subunit coordinates of AtFKBP53 NTD. The structures of nucleoplasmin family proteins were identified as the nearest structural neighbours (Supplementary Table S2). AtFKBP53 NTD aligns reasonably well with all known nucleoplasmin structures, with differences being observed primarily in the orientation of the flexible loop regions (Supplementary Figure S5). Minor variations could be observed in the length, position, and orientation of the β strands. The only striking difference was the presence of the short 3_{10} helix in AtFKBP53 NTD that is absent in all other known NPM structures. The presence of 3_{10} helix seems to stabilize the loop region be-

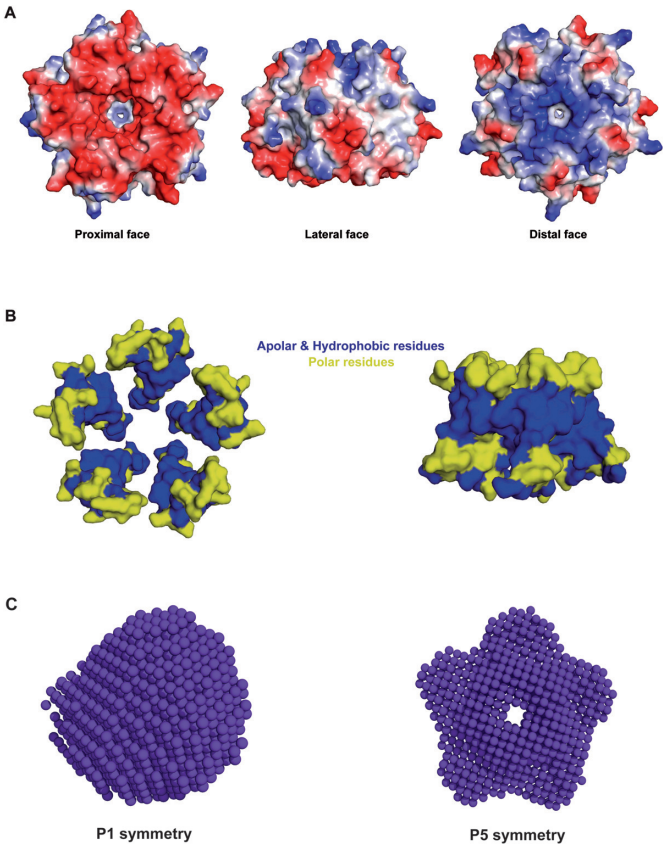

Figure 3. Surface charge, apolar and hydrophobic residue distribution and oligomeric status of AtFKBP53 NTD pentamer. (**A**) The electrostatic surface potential of AtFKBP53 NTD pentamer in three different orientations shows its proximal, lateral and distal faces. The figures were generated using PyMOL and coloured linearly from red (–kT) to blue (+kT). The proximal and distal faces reveal a relative abundance of acidic and basic charges, respectively. (**B**) The beta-sheets forming the inner and the outer cores of AtFKBP53 NTD pentamer in different orientations have been depicted in surface representation in yellow, showing the distribution of apolar and hydrophobic residues in blue, forming a concentric ring-like network, facing each other and thereby stabilizing the pentamer structure. (**C**) AtFKBP53 NTD envelope generated from the SAXS scattering profile using the ATSAS software DAMMIF and DAMAVER in P1 and P5 symmetries.

tween the strands β2 and β3; whereas, the corresponding loop region has a disordered acidic tract in the structure of XlNPM1, DmNLP, XlNO38 and HsNPM1 (21–24). AtFKBP53 NTD aligned best with *D. melanogaster* FKBP39-NLP with an RMSD of 1.6.

The surface charge distribution of AtFKBP53 NTD (Figure 3A) appeared different from that of other known nucleoplasmin structures (Supplementary Figure S6). The acidic stretch (DDDDE) of AtFKBP53 NTD in its proximal face is located between strands β6 and β7, in contrast to other known nucleoplasmin structures, where a similar acidic stretch is present on the same face, but between β2 and β3 strands. The distribution of residues of this acidic stretch makes the proximal face of the AtFKBP53 NTD entirely negatively charged. The proximal face of other nucleoplasmin structures, except HsNPM2 and DmFKBP39 NLP, have a net negative charge, but much less compared to what is observed for AtFKBP53 NTD (Supplementary Figure S6). It is worth mentioning here that it is the acidic proximal face of nucleoplasmins that could allow a strong interaction with the basic histones. Therefore, an abundance of negative charge in this face of AtFKBP53 supports the possibility of an efficient histone interaction. The distal face of the pentamer, however, revealed a net basic charge (Figure 3A).

AtFKBP53 NTD pentamer is highly stable

Studies have illustrated that the distribution of apolar and hydrophobic residues within the pentameric core plays a significant role in providing high thermostability to nucleoplasmins such as XlNPM, DmNLP, XlNO38 NPM and HsNPM2 (21–24,60). The distribution of apolar residues in the primary sequence of AtFKBP53 NTD revealed a pattern similar to other nucleoplasmins (Supplementary Figure S7A). Like other reported nucleoplasmin structures (21–24), the apolar residues located in the interfacial region of the five monomers of AtFKBP53 NTD pentamer form a concentric ring mediated by hydrophobic interactions. When the beta-sheets forming the inner and outer core of the pentameric AtFKBP53 NTD structure are observed separately in a surface view, it becomes evident that the outer face of the inner core and the inner face of the outer core, that face each other are lined with apolar and hydrophobic residues, adding strength to the whole structure (Figure 3B). The analytical SEC of AtFKBP53 NTD subjected to high temperatures, high salt and denaturing conditions, separately, showed the pentamer to elute at the same volume as the untreated control sample with only minimal reduction in the peak intensities (Supplementary Figure S7B–D). The results indicate AtFKBP53 NTD pentamer to be reasonably stable and resistant to high temperatures, high concentrations of salt, as well as the presence of a denaturing agent.

AtFKBP53 NTD exists in a pentamer in solution, typical for nucleoplasmins

All studied nucleoplasmins are known to exist in higher oligomeric states, usually as a stable pentamer (60). The analytical SEC profile of AtFKBP53 NTD at 300 mM NaCl, suggested that the domain exists as a pentamer; eluting at a column volume corresponding to a molecular mass of 55 kDa, the theoretical molecular mass of the monomer being 11 kDa (Supplementary Figure S8A). However, upon lowering the salt concentration to 100 mM NaCl, the chromatogram revealed the presence of pentameric and decameric conformations, with the significant proportion of AtFKBP53 NTD remaining as a pentamer (Supplementary Figure S8B). This is also in accordance with earlier reports, which suggest that the decameric form is also an active conformation for nucleoplasmins, required for assembling histone octamers (21,24).

To endorse our result, we carried out small-angle X-ray scattering (SAXS) experiment for AtFKBP53 NTD, The Porod molecular weight and volume calculated from the X-ray scattering patterns also indicated a pentameric conformation. The Kratky plot, Guinier analysis curve and computed distance distribution p(r) plot, all showed the presence of a well-folded globular protein conformation, free of

any aggregation (Supplementary Figure S8C). The *ab initio* average model generated from all the models in P1 and P5 symmetry neatly fitted the experimental data (Figure 3C). The experimental model validation with that of the crystal structure showed a perfect fit, yielding a chi-square value of 1.211. The existence of AtFKBP53 NTD as a pentamer was thereby confirmed. The SAXS data collection details and parameters from the scattering curves are given in Supplementary Table S3.

AtFKBP53 NTD binds to both H3/H4 and H2A/H2B

AtFKBP53 has already been reported to interact with histone H3, wherein only its N-terminal domain is indispensable and sufficient for the interaction (14). However, the interaction of the protein with other histones has not been reported. Histone chaperones usually associate with histone oligomers and not individual histones. Moreover, all the nucleoplasmins studied so far interact with histone H2A/H2B and/or H3/H4 (21,23,28,29,61). Hence, we were interested in investigating for the interaction of both AtFKBP53 NTD and AtFKBP53 FKBD with H2A/H2B and H3/H4 histone complexes, separately.

For binding assays, we used a slightly longer stretch of the N-terminal domain of AtFKBP53 (residues 1–112), to avoid the overlapping peaks in size exclusion chromatography profiles and the indistinguishable bands in SDS-PAGE, as described later. Also, in the process of making a longer construct, we included the second acidic stretch (A2) which would possibly improve its histone-binding abilities. We first tested the interaction of the domain with histone oligomers by performing *in vitro* pull-down assays using Nickel NTA resin (Supplementary Figure S9A). Purified His_6-tagged AtFKBP53 NTD and AtFKBP53 CTD were incubated with untagged H2A/H2B or H3/H4 complexes, separately, followed by immobilization on the beads. Both H2A/H2B and H3/H4 complexes co-eluted with AtFKBP53 NTD, which indicated that AtFKBP53 NTD was capable of binding to both H2A/H2B and H3/H4. AtFKBP53 CTD did not show any interaction with both the histone oligomers (Supplementary Figure S9A). However, we do not rule out the possibility for a transient interaction wherein the C-terminal domain (FKBD) performs the role of a PPIase on histone substrates. This would need further verification.

To validate the interaction of AtFKBP53 NTD with H2A/H2B and H3/H4, and also to determine the interaction stoichiometry, we performed analytical SEC experiments. The shift in the elution volumes of the complexes in analytical SEC and further SDS-PAGE analyses of the peak fractions showed that AtFKBP53 NTD indeed interacts with H2A/H2B and H3/H4, independently (Figure 4A). However, the stoichiometry of binding could not be precisely determined from the size-exclusion chromatogram as the peak shift would depend not only on the molecular mass of the complex but also on its shape and more so for non-globular proteins/complexes. We sought to validate the binding stoichiometry further with sedimentation velocity analytical ultracentrifugation (SV-AUC) experiments using a continuous size distribution model (62), which revealed AtFKBP53 NTD–H2A/H2B to have a sedimentation coefficient (S) value of 5.4S that corresponds to a molecular mass of 104 kDa, the size expected for a pentamer of AtFKBP53 NTD bound to one H2A/H2B dimer. Similarly, for AtFKBP53 NTD–H3/H4, the major peak gave a sedimentation coefficient (*S*) value of 7.35S that corresponds to a molecular mass of 129 kDa, the size expected for a pentamer of AtFKBP53 NTD bound to H3/H4 tetramer. The above results thus demonstrate that AtFKBP53 NTD can interact specifically with both H2A/H2B and H3/H4, like other known nucleoplasmins and confirms AtFKBP53NTD to be a histone chaperone belonging to the family of nucleoplasmins. The observed molecular masses had less than 10% error as compared to theoretical molecular mass. The data from SV-AUC analysis using SEDFIT software has been reported in (Figure 4B, Supplementary Figure S9B, C and Supplementary Table S4).

To further explore the binding stoichiometry and to determine the thermodynamic parameters of the interaction between AtFKBP53 NTD and histone oligomers, we used isothermal titration calorimetry (ITC) (Figure 4C). Upon titrating AtFKBP53 NTD with H2A/H2B and H3/H4 separately, an endothermic reaction was observed in both the cases. The calculated thermodynamic parameters are shown in Figure 4C (right panel). In both the cases, the reaction was entropically driven with ($-T\Delta S$) of −21.3 kcal/mol and a K_d of 0.50 ± 0.09 μM for H2A/H2B, while having a ($-T\Delta S$) of −27.6 kcal/mol and a K_d of 0.87 ± 0.1 μM for H3/H4. Both the interactions showed a 1:1 binding stoichiometry (*n*) in line with the other results. A large positive change in entropy (ΔS) is known to occur due to conformational changes taking place between interacting partners upon binding and also release of ordered water molecules in bulk solvent due to hydrophobic interactions between them (63–65). Both the interactions thus appeared to be driven by hydrophobic interactions; although hydrogen bond/electrostatic interactions also seem to play a role in the interaction (Figure 4C, right panel). The oligomeric conformation of the H3/H4 in the experimental condition was evaluated using analytical SEC and cross-linking, indicating the majority of the protein to be present in tetrameric conformation. (Supplementary Figure S10A, B) and also it has previously been reported that in low salt buffer conditions, H3/H4 at a concentration >1 μM exists primarily in a tetrameric conformation (66). The K_d values from the titration experiments indicate that the AtFKBP53 NTD pentamer seems to have a slightly higher affinity for H2A/H2B as opposed to H3/H4, which does not appear very significant.

The previous report on AtFKBP53 has shown its interaction only with histone H3. In contrast, our ITC experiments show AtFKBP53 NTD to have a higher binding affinity for H2A/H2B than H3/H4. We, therefore, performed an additional pull-down assay to further validate our observations. In this assay, separate experiments were performed, where all binding sites on His_6-tagged pentameric AtFKBP53 NTD were saturated by incubating it with either untagged H3/H4 (Figure 5A, left panel) or H2A/H2B (Figure 5A, right panel) in a 1:3 ratio followed by titration with five times excess concentrations of H2A/H2B or H3/H4, respectively. In both the experiments, upon elution, AtFKBP53 NTD came together with H2A/H2B and

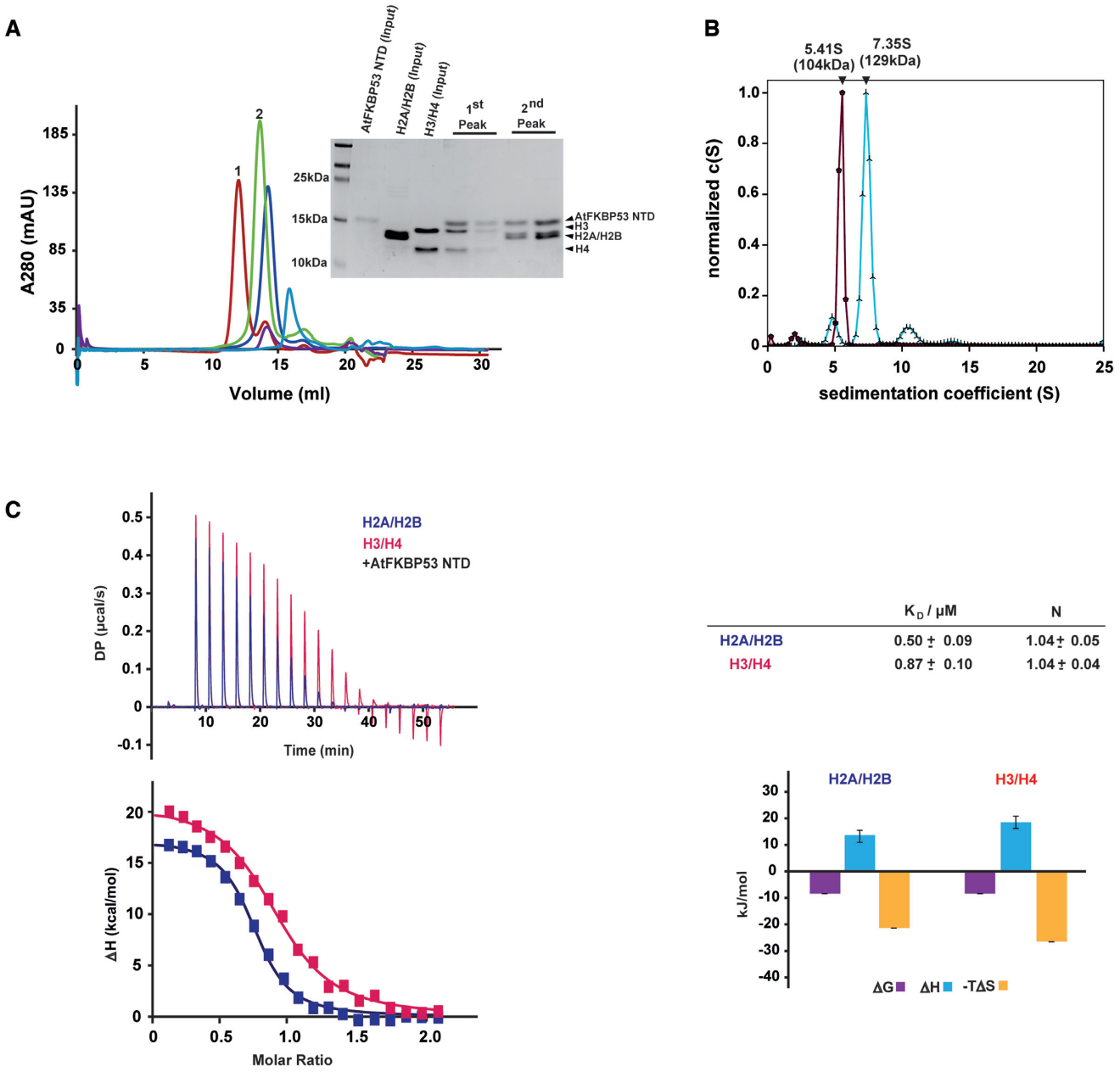

Figure 4. AtFKBP53 NTD pentamer interacts with H2A/H2B and H3/H4. (**A**). Analytical size-exclusion chromatography profile of AtFKBP53 NTD (purple), H2A/H2B (light blue), H3/H4 (violet), AtFKBP53 NTD/H2A/H2B mixture (green) and AtFKBP53 NTD/H3/H4 mixture (red) indicating stable complex formation. 18% SDS-PAGE gel showing the peak fractions obtained from size-exclusion chromatography, confirming complex formation (inset). (**B**) Analytical ultracentrifugation distance distribution *c*(*S*) versus sedimentation coefficient (*S*) plot obtained from SEDFIT software for AtFKBP53 NTD/H2A/H2B complex (dark red) and AtFKBP53 NTD/H3/H4 complex (sky blue). (**C**) Calorimetric titration of AtFKBP53 NTD with H2A/H2B and H3/H4 via ITC at 25°C. In the left upper panel heat changes of injections of AtFKBP53 NTD to H2A/H2B (blue) and H3/H4 (red) are shown. The resulting isotherms fitted with one-set of site binding model were shown in the left lower panel. The upper right panel shows the best fit values and fitting errors while the lower-left panel shows the graphical representation of thermodynamic parameters from the titration experiments. The data were acquired in a buffer containing 20 mM PIPES (pH 7.4) and 300 mM NaCl.

H3/H4, which suggested the presence of separate binding sites on AtFKBP53 NTD for the two histone oligomers. To support our findings, we performed an analytical SEC, which showed an early elution peak for AtFKBP53 NTD in complex with both H2A/H2B and H3/H4, in comparison to the peaks of the individual complexes AtFKBP53 NTD-H2A/H2B and AtFKBP53 NTD-H3/H4 (Figure 5B, left panel). The collected peak fractions for the complex showed the presence of all the five components when analysed on an 18% SDS-PAGE gel (Figure 5B, right panel). This demonstrates the possibility of AtFKBP53 NTD binding to H2A/H2B and H3/H4 at two different sites, similar to XlNPM, as has been suggested earlier (29).

The ITC experiment showed the binding of both histone oligomers H2A/H2B or H3/H4 to AtFKBP53 NTD to be driven by hydrophobic interactions as has been re-

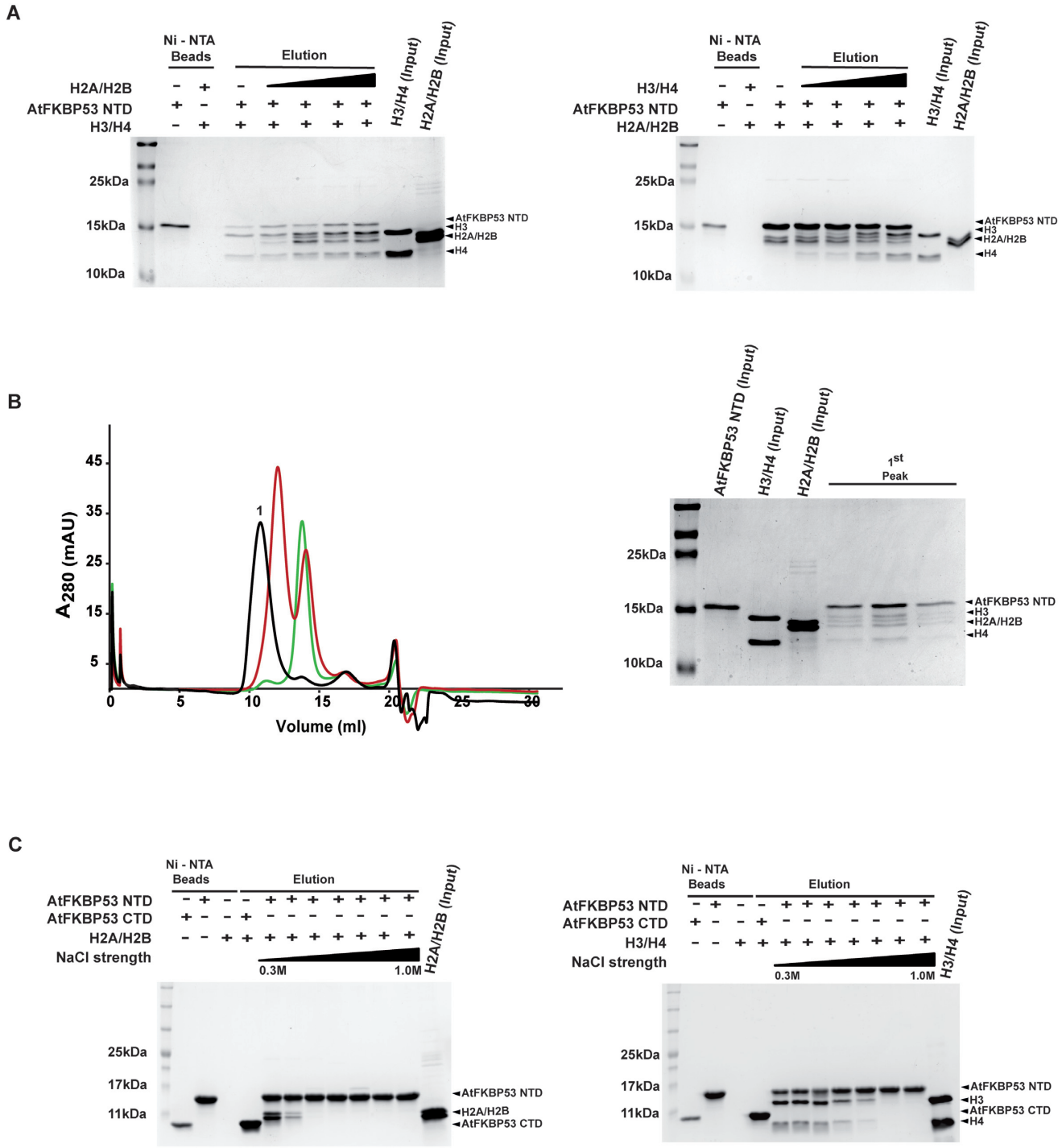

Figure 5. AtFKBP53 NTD can bind to both H2A/H2B and H3/H4, simultaneously. (**A**) The sequential binding experiment, wherein the left panel shows eluted fractions of saturated AtFKBP53 NTD–H3/H4 complex titrated with an increasing gradient of H2A/H2B, run on an 18% SDS PAGE gel. The right panel shows the 18% SDS PAGE gel image for the eluted fractions of saturated AtFKBP53 NTD–H2A/H2B complex, titrated with an increasing gradient of H3/H4. (**B**) Analytical size-exclusion chromatogram of AtFKBP53 NTD–H2A/H2B complex (green), AtFKBP53 NTD–H3/H4 complex (red) and AtFKBP53 NTD–H2A/H2B/H3/H4 complex (black). Collected peak fraction for AtFKBP53 NTD–H2A/H2B-H3/H4 complex analysed on an 18% SDS-PAGE gel (right panel) shows individual bands for all the components in the complex and confirms simultaneous binding of AtFKBP53 NTD to H2A/H2B and H3/H4. (**C**) Eluted fractions from separate pull-down experiments of AtFKBP53 NTD–H2A/H2B complex (left panel) and AtFKBP53 NTD–H3/H4 complex (right panel) performed with increasing salt concentrations (0.3–1.0 M) analysed on an 18% SDS-PAGE gel. The presence of both H2A/H2B and H3/H4 bound to AtFKBP53 NTD even at higher ionic strength conditions suggest a major role for hydrophobic interactions in stabilizing both the complexes. The intensity of the H2A/H2B bands at 0.5 M ionic strength suggests a role also for ionic interactions in stabilizing the complexes.

ported earlier (29,30). This was corroborated by a pull-down assay where several reactions were set up wherein His_6-tagged AtFKBP53 NTD was incubated with untagged H2A/H2B (Figure 5C, left panel) or H3/H4 (Figure 5C, right panel) with increasing salt concentration conditions. Upon elution, H2A/H2B dimer was found to interact with AtFKBP53 NTD up to 0.5 M NaCl concentration and H3/H4 up to 0.7 M NaCl concentration, suggesting that the binding of both the histone oligomers to AtFKBP53 NTD is driven by hydrophobic interactions. However, reduction in the intensity of the H2A/H2B bands, at 0.5 M NaCl suggests a more significant role for ionic interactions in stabilizing the complex. So it is possible that H2A/H2B interaction of the pentamer is mediated by the charged proximal face closer to the centre and H3/H4 interaction could happen next to H2A/H2B interaction site, having a significant contribution from the aromatic corner adjacent to the proximal face.

AtFKBP53 NTD is involved in nucleosome assembly and binds to preformed nucleosomes

Nucleoplasmins are known to be involved in chromatin assembly reactions (21,28,61,67,68). The ability of the protein to interact with H2A/H2B and H3/H4 shows it to play a role in histone binding and perhaps, nucleosome assembly process. Firstly, to investigate whether AtFKBP53 NTD mediates nucleosome assembly, we carried out plasmid supercoiling assay. When nucleosome forms on relaxed and closed circular DNA (rccDNA), it introduces negative supercoil that can be analysed on an agarose gel in terms of the super-helicity formed in the DNA. Indeed, AtFKBP53 NTD was seen to significantly introduce negative supercoiling in rccDNA, in the presence of H2A/H2B and H3/H4 in a dose-dependent manner. In contrast, AtFKBP53 NTD and histones alone did not induce supercoiling. In this experiment, AtFKBP53 CTD also did not show supercoiling activity in the presence of histones (Figure 6A). The above result indicates that AtFKBP53 NTD possesses nucleosome assembly activity like other nucleoplasmins. To explore its interaction with preformed nucleosome, we conducted electrophoretic mobility shift assay (EMSA) on reconstituted NCP incubated with increasing amounts of AtFKBP53 NTD pentamer, in the range of 1:1 to 1:5. We also looked at the binding ability of AtFKBP53 CTD to NCP when mixed in a 1:1 ratio, thinking it might interact with histones assembled in the NCP or to the DNA. Bovine serum albumin (BSA) was taken as a negative control to rule out the nonspecific interactions based on the fact that BSA has a theoretical isoelectric point (p*I*) close to AtFKBP53 NTD with an equal distribution of basic and acidic residues on its surface. From the above experiment, we observed a faint band corresponding to unbound NCP at 1:1 ratio, which was absent in higher ratios. We also noticed a decrease in the migration rate of NCP in the presence of AtFKBP53 NTD up to 1:2 ratio, after which no further change in the migration pattern was observed (Figure 6B). When the EMSA gel was further examined by Coomassie Brilliant Blue R250 staining, a band corresponding to the unbound AtFKBP53 NTD was found for the samples of NCP incubated with AtFKBP53 NTD pentamer in a 1:3 to 1:5 ratio (Supplementary Figure S11A). This indicated a specific interaction between NCP and AtFKBP53 NTD pentamer at 1:2 ratio. In contrast, AtFKBP53 FKBD and BSA did not affect the migration of NCP but showed mild precipitation in the wells, which might be due to non-specific interactions. To check for the specificity of the interaction, we incubated NCP with AtFKBP53 NTD pentamer at 1:2 ratio in increasing salt concentrations and conducted an EMSA analysis. The EMSA results showed a similar shift and migration pattern for the complex in all the salt concentrations we tried, indicating a specific interaction between AtFKBP53 NTD pentamer and NCP (Supplementary Figure S11B).

To confirm the specificity of the interaction between AtFKBP53 NTD pentamer and NCP, we performed SV-AUC experiments using a continuous size distribution model (Figure 6C; Supplementary Figure S11C; Supplementary Table S5). The NCP alone showed a sedimentation coefficient (*S*) value of 10.7*S* ($S_{20,w}$ 11*S*) that corresponded to a molecular mass of 214 kDa and NCP with AtFKBP53 NTD added in 1:2 and 1:3 ratio gave a higher sedimentation coefficient value of 11.8S that corresponds to a molecular mass of 303–308 kDa, the size expected for an NCP bound to two AtFKBP53 NTD pentamers. The observed molecular masses showed less than 10% error as compared to the theoretical molecular masses.

We carried out isothermal titration calorimetry experiments to confirm the stoichiometry of AtFKBP53 NTD pentamer and NCP while forming the complex. The binding isotherm was fitting with a sequential binding model having two binding sites. This confirmed the EMSA and AUC data, which also indicated the interaction between NCP and AtFKBP53 NTD to saturate at a 1:2 ratio. The K_d values for the two binding sites were found to be 0.18 ± 0.018 μM (K_{d1}) and 2.72 ± 0.17 μM (K_{d2}) (Figure 6D). This supports the formation of a stable complex between AtFKBP53 NTD pentamer, and NCP, wherein, one pentamer could be binding to each of the two faces of a nucleosome on its histone surface.

AtFKBP53 NTD and FKBD function independent of each other

Studies on *S. cerevisiae* Fpr4, an acidic histone chaperone containing a C-terminal FKBD, have shown that the removal of its FKBD greatly increases its histone chaperone activity, signifying an inhibitory role of this domain on histone chaperone activity (17). Analysis of charge distribution of AtFKBP53 FKBD (Figure 1D) and AtFKBP53 NTD (Figure 3A) revealed the former to be basic and the latter to be acidic on its one face. Thus we wanted to check whether there is any specific electrostatic interaction between the two domains, which in turn might have a role in regulating the histone-binding characteristics of the N-terminal nucleoplasmin domain. To confirm this, we performed analytical SEC of a mixture of the two individual domains in a 1:1 stoichiometric ratio, as well as the two domains individually. We observed that, even when mixed together, the two domains eluted separately at different volumes, corresponding to their individual molecular masses (Supplementary Figure S12). This indicated that the two domains do not form

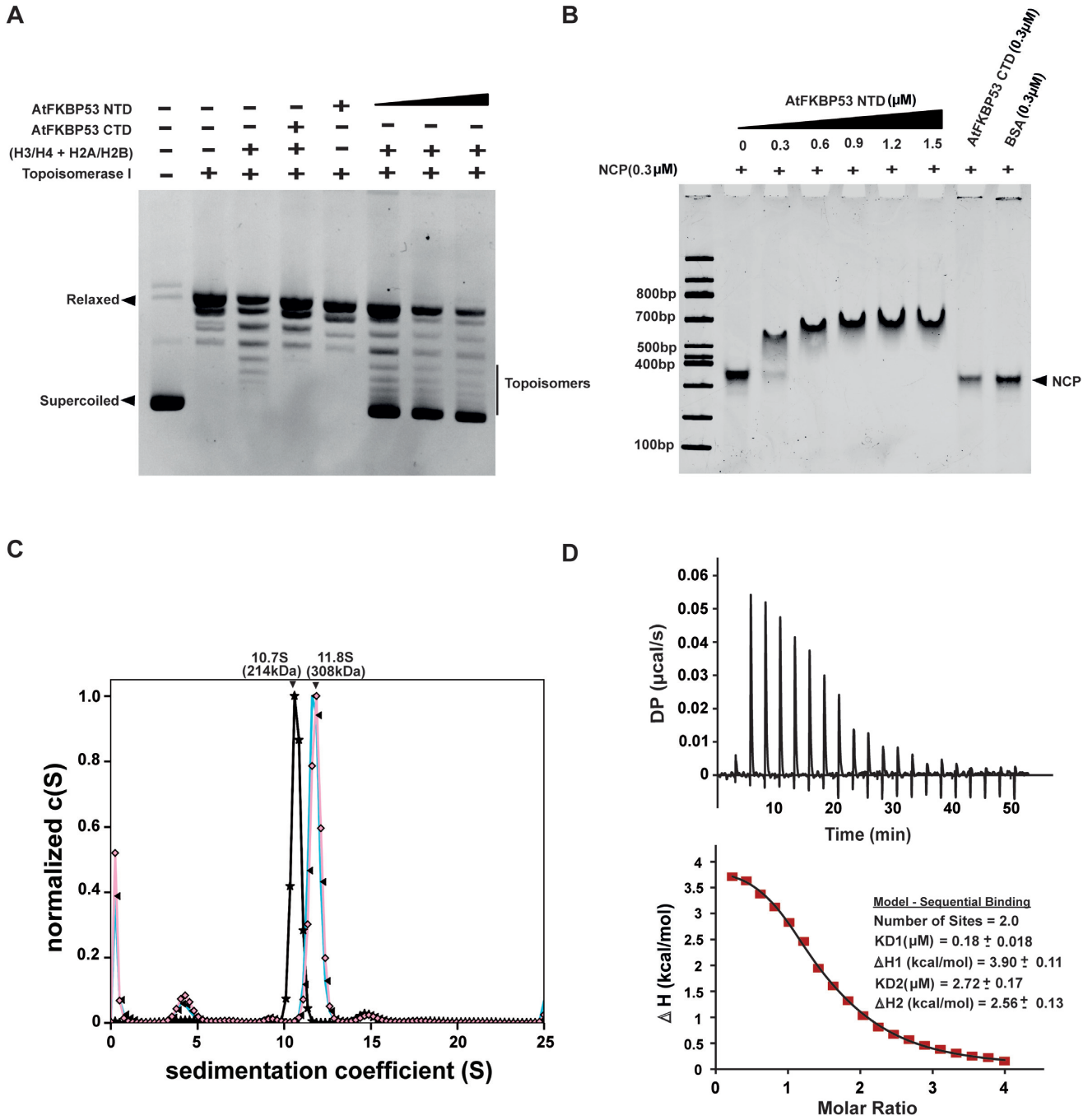

Figure 6. AtFKBP53 NTD is a functional histone chaperone and it interacts with NCP. (**A**) Supercoiling assay using relaxed closed circular (rcc) pUC19 plasmid (0.5 μg) incubated with histone H2A/H2B, H3/H4 and increasing amounts of AtFKBP53 NTD (1.0–3.0 μM). AtFKBP53 NTD shows supercoiling activity in the presence of histones and (rcc) pUC19 plasmid DNA, whereas AtFKBP53 FKBD did not show any supercoiling activity in the presence of histones and (rcc) pUC19. AtFKBP53 NTD and histones alone were also not able to induce supercoiling in rccPU19 DNA. (**B**) Electrophoretic mobility shift assay (EMSA) of NCP with AtFKBP53 NTD pentamer in incremental ratios ranging from 1:1 to 1:5 on a 6% Native-PAGE stained with ethidium bromide. NCP with AtFKBP53 CTD and BSA separately in 1:1 ratio were run as controls. The gel showed that AtFKBP53 NTD pentamer binds to NCP, and the reaction appears to reach saturation at about 1:2 ratio, whereas AtFKBP53 FKBD and BSA did not show any specific interaction with NCP. (**C**) SV-AUC distance distribution $c(S)$ versus sedimentation coefficient (S) plot obtained from SEDFIT software for NCP (black), a mixture of NCP and AtFKBP53 NTD pentamer in 1:2 ratio (sky blue) and a mixture of NCP and AtFKBP53 NTD pentamer in 1:3 ratio (light pink). (**D**) Calorimetric titration of AtFKBP53 NTD pentamer with NCP at 25°C. In the right upper panel, heat changes from injections of AtFKBP53 NTD into NCP (black) are shown. In the lower panel, the resulting isotherms (fitted with a sequential binding model) are shown. The actual experimental positions are represented as a black line and the fitted positions are represented as red dots. The dissociation constant value (K_d) and thermodynamic parameters are shown as an inset in the lower panel. Data were acquired in 20 mM Tris (pH 7.5), 50 mM NaCl and 1.0 mM β-mercaptoethanol.

a discrete complex with each other and that they might perform independent functions.

DISCUSSION

This forms the first detailed structural and functional characterization report of a nuclear-localized FKBP-type immunophilin from a plant. Our work shows that the C-terminal domain of AtFKBP53 exists as a monomer with a typical FKBD fold and that it is a functional PPIase. A previous report has shown AtFKBP53 to be a histone chaperone, involved in the regulation of ribosome biogenesis, wherein, the FKBD or the PPIase domain is dispensable for histone H3 binding and histone chaperoning activity, both (14). Our study confirms that the C-terminal FKBD of AtFKBP53 does not show any interaction with H2A/H2B or H3/H4 *in vitro*, thereby indicating that the FKBD does not play any role in its histone chaperoning function and that it is the N-terminal nucleoplasmin domain that does the function of a histone chaperone. It is worth mentioning here that the previous report of full-length AtFKBP53 and its N-terminal domain could identify binding only to histone H3 (14), may be due to the fact that the authors had used GST-tagged AtFKBP53 for the interaction studies. From our experiments, we have found the presence of an N-terminal GST tag to prevent the formation of pentameric AtFKBP53 NTD, restricting it in a dimeric state (data not shown). Therefore, the pentameric oligomeric conformation of the protein may be necessary for the interaction with H2A/H2B. One could also not rule out the possibility that the GST tag might have occluded the H2A/H2B binding site of the nucleoplasmin in that study.

Nucleoplasmins from the animal kingdom have been structurally characterized. However, this forms the first report of a plant nucleoplasmin structure. Through our study, we confirm that the N-terminal domain of AtFKBP53 exists necessarily as a pentamer with the classical nucleoplasmin-fold, showing close similarity with other structurally characterized nucleoplasmins, albeit with a very low sequence identity. Size-exclusion chromatography data suggest the presence of decameric conformations in low salt concentrations that may have a physiological relevance similar to other structurally characterized nucleoplasmin decamers such as XlNPM, XlNO38-NPM and HsNPM1 (21,23,25). Comparison of the crystal structures of XlNPM and AtFKBP53 NTD shows that the latter lacks both the AKDE motif and the previously reported Lys82 of the K-loop present in XlNPM, responsible for decamer formation through pentamer–pentamer interfacial interactions between Asp58 and Glu59 of the AKDE motif in one pentamer with Lys82 and Lys57 present in the other pentamer, respectively (21). However, AtFKBP53 has a Glu residue in place of Asp58 and also a Lys62 residue located in the K loop and that might still mediate weak inter-pentameric interactions leading to decamer formation that we see only under low salt conditions. The crystal packing for AtFKBP53 NTD had ten molecules in the asymmetric unit. But the two pentamers were not packed in a decameric conformation.

Like most of the nucleoplasmin family proteins, which contain acidic stretches both in the nucleoplasmin core domain, and in the C-terminal tail (15,21–23,25,26,31), AtFKBP53 also possesses some acidic stretches along its length (14). A comparison of its domain organization and acidic stretch distribution with structurally known nucleoplasmins revealed that a short, five residue-long acidic stretch (DDDDE) corresponding to residues 73–77 (denoted as A1) is present at the core domain end of AtFKBP53 (Supplementary Figure S13). However, in all other known nucleoplasmins, the acidic stretch is present at the start of the core domain (Supplementary Figure S13). Opposed to nucleoplasmins which usually have two acidic stretches of varying length in the tail region, C-terminal to the core domain, AtFKBP53 has three acidic stretches denoted as A2 (residues 100–141), A3 (residues 163–169) and A4 (residues 210–215), respectively, in the order of their occurrence in the sequence (Supplementary Figure S13). The presence of an additional acidic tract A4 in contrast to other nucleoplasmins, may suggest a stronger or more specific histone-binding ability for AtFKBP53. Indeed, the surface charge distribution of AtFKBP53 NTD shows the proximal face, which is previously reported to interact with the histones (69,70), to be highly negatively charged, much more in comparison to other nucleoplasmins (15,21–26).

Interaction studies with histone complexes showed that AtFKBP53 NTD interacts with both H2A/H2B and H3/H4 with moderate affinity. A previous study on H2A/H2B interaction with recombinant full-length XlNPM and recombinant XlNPM core, using ITC, reported K_d values of 150 nM and 1 μM, respectively (30). In the current work, AtFKBP53 NTD interaction with H2A/H2B through ITC has yielded a K_d value of 500 nM and an interaction stoichiometry similar to that of XlNPM core (30). In another report, H2A/H2B interactions with the recombinant forms of full-length and core XlNPM, as well as H3/H4 tetramer interaction with the recombinant full-length XlNPM have been studied using flourimetry (28). The affinity values for these constructs with H2A/H2B and H3/H4 tetramer have been reported to be much higher than what we observe for AtFKBP53 NTD (28). The variation observed in K_d values could be due to the inherent differences between the two proteins and also owing to the fact that two different techniques were employed to study the interactions.

The salt gradient based pull-down assays and ITC revealed the interactions of AtFKBP53 NTD with both H2A/H2B and H3/H4 to be driven by hydrophobic contacts, with contribution from electrostatic interactions. This bears resemblance to the previous reports on recombinant *X. laevis* nucleoplasmin interaction with histone oligomers (29,30). However, the salt gradient data suggested that the contribution from electrostatic interactions was more in the case of H2A/H2B interaction with ATFKBP53 NTD. Separately, sequential binding assays suggest that AtFKBP53 NTD may be accommodating H2A/H2B and H3/H4 at two different binding sites.

Further, we have observed that AtFKBP53 NTD binds to preformed nucleosomes. A recent cryo-electron microscopy report has shown that two pentamers of *X. laevis* egg nucleoplasmin can bind specifically to a histone octamer, forming an elongated structure, wherein, the nucleoplasmin tails use the interacting surface on octamer similar to the DNA in

a nucleosome context (71). The complex we got for the AtFKBP53 NTD pentamer with nucleosome show a similar stoichiometry. However, in the absence of structural information on AtFKBP53 NTD in complex with nucleosome, it would be too preliminary to compare our findings with the available cryo-electron microscopy data for the *X. laevis* egg nucleoplasmin in complex with histone octamer (71).

The measured affinity of AtFKBP53 NTD for histones H2A/H2B (K_d = 0.50 μM) and H3/H4 (K_d = 0.87 μM) is much lower than the measured affinity between histones and '601' DNA (72), which might restrict AtFKBP53 NTD-mediated disassembly of nucleosomes. This also suggests the importance of other factors that might be playing a role in nucleosome disassembly activity of AtFKBP53 NTD if any, like post-translational modifications of histones (Eg: K56 of H3), which in turn might aid in weakening the binding interaction between histones and DNA (72). Separately, there could be associated factors which, when recruited by AtFKBP53 NTD, would perform nucleosome disassembly (67). Detailed investigations are required to throw light on these avenues.

In AtFKBP53 NTD pentamer structure, Cys56 of β5 and Cys66 of β6 of one monomer and Cys65' of β6 from the adjacent monomer come moderately close. This feature is unique to AtFKBP53 NTD and is not present in any other nucleoplasmins that have been structurally characterized. Cys56 and Cys66 seem to be conserved across the putative FKBP53 proteins from the various plant species, whereas, Cys65 which is not conserved across the spectrum is replaced by either a Ser or a Thr residue in other plant species (Supplementary Figure S14A). Cys56 and Cys66 are 3.6 Å apart in AtFKBP53 NTD structure (Supplementary Figure S14B) and reveal possible intra-subunit disulphide bond formation, which along with the hydrophobic and apolar residue distribution might further contribute to the stability of the pentamer as is evident from the thermal and chemical denaturation experiments. The physiological relevance of such stabilization remains to be understood in nucleoplasmins although, a study does suggest that the stabilization helps to compensate for the destabilizing effect of the multiple phosphorylations that occur in the tail region and the flexible portions of the core domain to drive the protein into an active state (60). In addition to AtFKBP53, another functionally overlapping chaperone, namely AtFKBP43, is also known to exist in *A. thaliana*. However, structural characterization of the same has not been carried out yet. Reports show that knocking down either AtFKBP53 or AtFKBP43 does not show any visible defects in transgenic plants (14), suggesting that they may be functionally compensating each other. Also, the involvement of other histone chaperones, with similar or interlinked functions, cannot be ruled out.

Like some other nucleoplasmins, AtFKBP53 NTD could also negatively supercoil closed circular plasmid in the presence of histones, confirming its role in nucleosome assembly (37,73). During our expression and purification attempts for full-length AtFKBP53, the protein was found to bind to bacterial ribosomal protein L2 (Supplementary Figure S15), which is highly conserved across all kingdoms and is known to have a role in ribosomal subunit association and catalyzing peptide bond formation (74). Bacterial L2 has a 48% sequence identity with *A. thaliana* L2 protein while also being a basic protein, similar to histones, which indicates that AtFKBP53 might play a role in chaperoning ribosomal proteins as well, resembling HsB23 (nucleophosmin/NPM1) that helps in binding, storage and protection of ribosomal protein S9 (75). S9 is thought to play a significant role in ribosome biogenesis and the function of the mature ribosome, being able to bind to rRNA and having a role in cell proliferation and growth. This observation also supports the role of AtFKBP53 in regulating ribosome biogenesis, as has been reported previously (14).

Similar to AtFKBP53, the nucleolar FKBP Fpr4 from *S. cerevisiae,* having a C-terminal FKBD, possesses a histone chaperone function which is mediated through its N-terminus (76). However, unlike AtFKBP53, ScFpr4 FKBD has been shown to have an inhibitory role on its histone chaperoning activity through its tertiary structure, independent of its activity (17,76). The Fpr4 FKBD catalyses proline isomerization of histones H3 and H4, thereby affecting their lysine methylation status and regulation of gene expression (76). Whether or not, the FKBD of AtFKBP53 has a similar role in controlling the methylation status of histones, thereby regulating gene expression, requires further investigation.

The FKBP39 protein from *D. melanogaster* also shares similarities with AtFKBP53, both having an N-terminal nucleoplasmin domain and a C-terminal FKBD. DmFKBP39 is known to get expressed in all developmental stages with the highest expression in the early embryo and the ovary of adult flies, indicating its importance in rapidly dividing cells. Likewise, AtFKBP53 is reported to be expressed in all parts of the plant; however, with maximal expression in the rapidly dividing root tip (root apical meristem) and pollen (14). These proteins thus form a new subclass of nuclear FKBPs having a plausible role in histone binding, storage, and chromatin assembly with particular reference to ribosome biogenesis, wherein, their catalytic PPIase domain may or may not have a role to play in terms of H3 proline isomerization, subsequently affecting their methylation status. They may, therefore, act as part of a broader epigenetic switch that regulates the effective dosage of active rRNA genes in the system at a given time.

Based on the crystal structures of AtFKBP53 NTD and FKBD, and the predicted unstructured middle domain [PONDR VLXT prediction/IUPRED prediction (77,78)] (Supplementary Figure S16), we propose the full-length AtFKBP53 to have a 'spokes of a wheel' kind of structure (Supplementary Figure S17). The structure is characterized by a central pentameric core formed by the N-terminal nucleoplasmin domain of the five individual AtFKBP53 molecules, radiating out into five arms from the central core, formed by their respective unstructured middle domains. These arms finally end in their well-folded and functional C-terminal FKBDs or PPIase domains.

This work will act as a foundation for further studies towards the identification of physiologically relevant complexes of AtFKBP53. The characterization of such complex structures of AtFKBP53 with its binding partners such as histones and nucleosomes may reveal more details of the interactions that will help to better understand the mode of

action of this protein and its role in plant chromatin organization.

DATA AVAILABILITY

The structures have been deposited to PDB with the accession IDs 6J2M and 6J2Z (https://www.rcsb.org/).

SUPPLEMENTARY DATA

Supplementary Data are available at NAR Online.

ACKNOWLEDGEMENTS

Many thanks to Dr Curt A. Davey (NTU, Singapore) for providing the plasmid constructs of histones and '601' DNA; Dr Surendra C. Sabat (ILS, Bhubaneswar) for his guidance in performing PPIase assay; Dr Ashis Biswas (IIT, Bhubaneswar) for providing access to CD Polarimeter; Digvijay Singh Naruka and Dr Deepak Sharma (IMTECH, Chandigarh) and Dr Soumya De (IIT Kharagpur) for their help with AUC experiments; Dr Ashish Ganguly (IMTECH, Chandigarh) and the beamline scientists at BM29 (ESRF, Grenoble) for SAXS experiments; Dr Anthony Addlagatta of CSIR-IICT (Hyderabad) for providing access to in-house XRD facility for the preliminary characterization work; Dr Ravindra D. Makde, Dr Biplab Ghosh and Dr Ashwani Kumar (RRCAT, Indore) for their help with synchrotron XRD data collection at the PX beamline BL21; Dr Babu A. Manjasetty for his help with synchrotron XRD data collection at ESRF BM14 beamline; Dr Deepak T. Nair (RCB, Faridabad) for his help in arranging and coordinating ESRF trips. The authors would also thank their colleagues in ILS - Sudeshna Sen for her help with histone expression work; Chinmayee Mohapatra, Manas Jagdev and Ruchir Bobde for SAXS data collection; Ashish Kumar and Rajivgandhi S for X-ray data collection and AUC experiments; Debasish Deb for all the scientific discussions pertaining to this manuscript; Dr Narottam Acharya and Dr V. Arun Nagaraj for their critical comments about the manuscript. We wish to dedicate this manuscript to Dr Kunchithapadam Swaminathan (NUS, Singapore) for all the motivation and positive energy he has provided us.
Author contributions: A.K.S. carried out all the experiments, analyzed data and wrote the manuscript. A.D. analyzed data, organized and wrote the manuscript. J.C. carried out the structure solution of AtFKBP53 NTD. S.L. was involved in conceiving the project and provided the initial expression constructs. D.V. envisaged the project, planned and guided the experiments and wrote the manuscript.

FUNDING

Intramural support to D.V. from the Institute of Life Sciences, Bhubaneswar; extramural grants to D.V. from the Science and Engineering Research Board, Government of India [EMR/2014/000070 and CRG/2018/000695/PS]; Extramural grant to D.V. from the Department of Biotechnology, Ministry of Science and Technology, Government of India [BT/PR10374/MED/29/820/2013]; The data collection at ESRF BM14 beamline and BioSAXS beamline BM29 were supported by the EMBL-India consortium and the ESRF Access Program [BT/INF/22/SP22660/2017] by the Department of Biotechnology, Ministry of Science and Technology, Government of India; A.K.S. was supported by the fellowship program DBT-JRF from the Department of Biotechnology, Ministry of Science and Technology, Government of India; A.D. was supported by a National Post-Doctoral Fellowship (N-PDF) from Science and Engineering Research Board, Government of India. Funding for open access charge: Institutional Support (Institute of Life Sciences, Bhubaneswar).
Conflict of interest statement. None declared.

REFERENCES

1. Galat,A. (2003) Peptidylprolyl cis/trans isomerases (immunophilins): biological diversity–targets–functions. *Curr. Top. Med. Chem.*, **3**, 1315–1347.
2. Gothel,S.F. and Marahiel,M.A. (1999) Peptidyl-prolyl cis-trans isomerases, a superfamily of ubiquitous folding catalysts. *Cell Mol. Life Sci.*, **55**, 423–436.
3. Hamilton,G.S. and Steiner,J.P. (1998) Immunophilins: beyond immunosuppression. *J. Med. Chem.*, **41**, 5119–5143.
4. Siekierka,J.J., Wiederrecht,G., Greulich,H., Boulton,D., Hung,S.H., Cryan,J., Hodges,P.J. and Sigal,N.H. (1990) The cytosolic-binding protein for the immunosuppressant FK-506 is both a ubiquitous and highly conserved peptidyl-prolyl cis-trans isomerase. *J. Biol. Chem.*, **265**, 21011–21015.
5. Kang,C.B., Hong,Y., Dhe-Paganon,S. and Yoon,H.S. (2008) FKBP family proteins: immunophilins with versatile biological functions. *Neurosignals*, **16**, 318–325.
6. Ghartey-Kwansah,G., Li,Z., Feng,R., Wang,L., Zhou,X., Chen,F.Z., Xu,M.M., Jones,O., Mu,Y., Chen,S. *et al.* (2018) Comparative analysis of FKBP family protein: evaluation, structure, and function in mammals and Drosophila melanogaster. *BMC Dev. Biol.*, **18**, 7.
7. Bonner,J.M. and Boulianne,G.L. (2017) Diverse structures, functions and uses of FK506 binding proteins. *Cell Signal.*, **38**, 97–105.
8. Yao,Y.L., Liang,Y.C., Huang,H.H. and Yang,W.M. (2011) FKBPs in chromatin modification and cancer. *Curr. Opin. Pharmacol.*, **11**, 301–307.
9. Schiene-Fischer,C. (2015) Multidomain peptidyl prolyl cis/trans isomerases. *Biochim. Biophys. Acta*, **1850**, 2005–2016.
10. Vasudevan,D., Gopalan,G., Kumar,A., Garcia,V.J., Luan,S. and Swaminathan,K. (2015) Plant immunophilins: a review of their structure-function relationship. *Biochim. Biophys. Acta*, **1850**, 2145–2158.
11. Gollan,P.J., Bhave,M. and Aro,E.M. (2012) The FKBP families of higher plants: exploring the structures and functions of protein interaction specialists. *FEBS Lett.*, **586**, 3539–3547.
12. He,Z., Li,L. and Luan,S. (2004) Immunophilins and parvulins. Superfamily of peptidyl prolyl isomerases in Arabidopsis. *Plant Physiol.*, **134**, 1248–1267.
13. Geisler,M. and Bailly,A. (2007) Tete-a-tete: the function of FKBPs in plant development. *Trends Plant Sci.*, **12**, 465–473.
14. Li,H. and Luan,S. (2010) AtFKBP53 is a histone chaperone required for repression of ribosomal RNA gene expression in Arabidopsis. *Cell Res.*, **20**, 357–366.
15. Edlich-Muth,C., Artero,J.B., Callow,P., Przewloka,M.R., Watson,A.A., Zhang,W., Glover,D.M., Debski,J., Dadlez,M., Round,A.R. *et al.* (2015) The pentameric nucleoplasmin fold is present in Drosophila FKBP39 and a large number of chromatin-related proteins. *J. Mol. Biol.*, **427**, 1949–1963.
16. Park,S.K., Xiao,H. and Lei,M. (2014) Nuclear FKBPs, Fpr3 and Fpr4 affect genome-wide genes transcription. *Mol. Genet. Genomics*, **289**, 125–136.
17. Monneau,Y.R., Soufari,H., Nelson,C.J. and Mackereth,C.D. (2013) Structure and activity of the peptidyl-prolyl isomerase domain from the histone chaperone Fpr4 toward histone H3 proline isomerization. *J. Biol. Chem.*, **288**, 25826–25837.

18. Kuzuhara,T. and Horikoshi,M. (2004) A nuclear FK506-binding protein is a histone chaperone regulating rDNA silencing. *Nat. Struct. Mol. Biol.*, **11**, 275–283.
19. Shan,X., Xue,Z. and Melese,T. (1994) Yeast NPI46 encodes a novel prolyl cis-trans isomerase that is located in the nucleolus. *J. Cell Biol.*, **126**, 853–862.
20. Benton,B.M., Zang,J.H. and Thorner,J. (1994) A novel FK506- and rapamycin-binding protein (FPR3 gene product) in the yeast Saccharomyces cerevisiae is a proline rotamase localized to the nucleolus. *J. Cell Biol.*, **127**, 623–639.
21. Dutta,S., Akey,I.V., Dingwall,C., Hartman,K.L., Laue,T., Nolte,R.T., Head,J.F. and Akey,C.W. (2001) The crystal structure of nucleoplasmin-core: implications for histone binding and nucleosome assembly. *Mol. Cell*, **8**, 841–853.
22. Namboodiri,V.M., Dutta,S., Akey,I.V., Head,J.F. and Akey,C.W. (2003) The crystal structure of Drosophila NLP-core provides insight into pentamer formation and histone binding. *Structure*, **11**, 175–186.
23. Namboodiri,V.M., Akey,I.V., Schmidt-Zachmann,M.S., Head,J.F. and Akey,C.W. (2004) The structure and function of Xenopus NO38-core, a histone chaperone in the nucleolus. *Structure*, **12**, 2149–2160.
24. Platonova,O., Akey,I.V., Head,J.F. and Akey,C.W. (2011) Crystal structure and function of human nucleoplasmin (npm2): a histone chaperone in oocytes and embryos. *Biochemistry*, **50**, 8078–8089.
25. Lee,H.H., Kim,H.S., Kang,J.Y., Lee,B.I., Ha,J.Y., Yoon,H.J., Lim,S.O., Jung,G. and Suh,S.W. (2007) Crystal structure of human nucleophosmin-core reveals plasticity of the pentamer-pentamer interface. *Proteins*, **69**, 672–678.
26. Mitrea,D.M., Grace,C.R., Buljan,M., Yun,M.K., Pytel,N.J., Satumba,J., Nourse,A., Park,C.G., Madan Babu,M., White,S.W. *et al.* (2014) Structural polymorphism in the N-terminal oligomerization domain of NPM1. *Proc. Natl. Acad. Sci. U.S.A.*, **111**, 4466–4471.
27. Frehlick,L.J., Eirin-Lopez,J.M. and Ausio,J. (2007) New insights into the nucleophosmin/nucleoplasmin family of nuclear chaperones. *Bioessays*, **29**, 49–59.
28. Fernandez-Rivero,N., Franco,A., Velazquez-Campoy,A., Alonso,E., Muga,A. and Prado,A. (2016) A Quantitative Characterization of Nucleoplasmin/Histone Complexes Reveals Chaperone Versatility. *Sci. Rep.*, **6**, 32114.
29. Arnan,C., Saperas,N., Prieto,C., Chiva,M. and Ausio,J. (2003) Interaction of nucleoplasmin with core histones. *J. Biol. Chem.*, **278**, 31319–31324.
30. Taneva,S.G., Banuelos,S., Falces,J., Arregi,I., Muga,A., Konarev,P.V., Svergun,D.I., Velazquez-Campoy,A. and Urbaneja,M.A. (2009) A mechanism for histone chaperoning activity of nucleoplasmin: thermodynamic and structural models. *J. Mol. Biol.*, **393**, 448–463.
31. Prado,A., Ramos,I., Frehlick,L.J., Muga,A. and Ausio,J. (2004) Nucleoplasmin: a nuclear chaperone. *Biochem. Cell Biol.*, **82**, 437–445.
32. Warren,C., Matsui,T., Karp,J.M., Onikubo,T., Cahill,S., Brenowitz,M., Cowburn,D., Girvin,M. and Shechter,D. (2017) Dynamic intramolecular regulation of the histone chaperone nucleoplasmin controls histone binding and release. *Nat. Commun.*, **8**, 2215.
33. Luger,K., Rechsteiner,T.J. and Richmond,T.J. (1999) Preparation of nucleosome core particle from recombinant histones. *Methods Enzymol.*, **304**, 3–19.
34. Luger,K., Rechsteiner,T.J. and Richmond,T.J. (1999) Expression and purification of recombinant histones and nucleosome reconstitution. *Methods Mol. Biol.*, **119**, 1–16.
35. Vasudevan,D., Chua,E.Y. and Davey,C.A. (2010) Crystal structures of nucleosome core particles containing the '601' strong positioning sequence. *J. Mol. Biol.*, **403**, 1–10.
36. Whitmore,L. and Wallace,B.A. (2004) DICHROWEB, an online server for protein secondary structure analyses from circular dichroism spectroscopic data. *Nucleic Acids Res.*, **32**, W668–W673.
37. Okuwaki,M., Matsumoto,K., Tsujimoto,M. and Nagata,K. (2001) Function of nucleophosmin/B23, a nucleolar acidic protein, as a histone chaperone. *FEBS Lett.*, **506**, 272–276.
38. Zhang,M., Liu,H., Gao,Y., Zhu,Z., Chen,Z., Zheng,P., Xue,L., Li,J., Teng,M. and Niu,L. (2016) Structural Insights into the Association of Hif1 with Histones H2A-H2B Dimer and H3-H4 Tetramer. *Structure*, **24**, 1810–1820.
39. Takahashi,N., Hayano,T. and Suzuki,M. (1989) Peptidyl-prolyl cis-trans isomerase is the cyclosporin A-binding protein cyclophilin. *Nature*, **337**, 473–475.
40. Furutani,M., Iida,T., Yamano,S., Kamino,K. and Maruyama,T. (1998) Biochemical and genetic characterization of an FK506-sensitive peptidyl prolyl cis-trans isomerase from a thermophilic archaeon, Methanococcus thermolithotrophicus. *J. Bacteriol.*, **180**, 388–394.
41. J.Goldberg,R. (1953) Sedimentation in the Ultracentrifuge. *J. Phys. Chem*, **57**, 194–202.
42. Schuck,P. (2000) Size-distribution analysis of macromolecules by sedimentation velocity ultracentrifugation and lamm equation modeling. *Biophys. J.*, **78**, 1606–1619.
43. Franke,D., Petoukhov,M.V., Konarev,P.V., Panjkovich,A., Tuukkanen,A., Mertens,H.D.T., Kikhney,A.G., Hajizadeh,N.R., Franklin,J.M., Jeffries,C.M. *et al.* (2017) ATSAS 2.8: a comprehensive data analysis suite for small-angle scattering from macromolecular solutions. *J. Appl. Crystallogr.*, **50**, 1212–1225.
44. Franke,D. and Svergun,D.I. (2009) DAMMIF, a program for rapid ab-initio shape determination in small-angle scattering. *J. Appl. Crystallogr.*, **42**, 342–346.
45. Volkov,V.V. and Svergun,D.I. (2003) Uniqueness of ab-initio shape determination in small-angle scattering. *J. Appl. Crystallogr.*, **36**, 860–864.
46. Svergun,D.I., Barberato,C. and Koch,M.H.J. (1995) CRYSOL - a program to evaluate X-ray solution scattering of biological macromolecules from atomic coordinates. *J. Appl. Crystallogr.*, **28**, 768–773.
47. Terakura,S., Ueno,Y., Tagami,H., Kitakura,S., Machida,C., Wabiko,H., Aiba,H., Otten,L., Tsukagoshi,H., Nakamura,K. *et al.* (2007) An oncoprotein from the plant pathogen agrobacterium has histone chaperone-like activity. *Plant Cell*, **19**, 2855–2865.
48. Fujii-Nakata,T., Ishimi,Y., Okuda,A. and Kikuchi,A. (1992) Functional analysis of nucleosome assembly protein, NAP-1. The negatively charged COOH-terminal region is not necessary for the intrinsic assembly activity. *J. Biol. Chem.*, **267**, 20980–20986.
49. Battye,T.G., Kontogiannis,L., Johnson,O., Powell,H.R. and Leslie,A.G. (2011) iMOSFLM: a new graphical interface for diffraction-image processing with MOSFLM. *Acta Crystallogr. D. Biol. Crystallogr.*, **67**, 271–281.
50. Evans,P.R. and Murshudov,G.N. (2013) How good are my data and what is the resolution? *Acta Crystallogr. D. Biol. Crystallogr.*, **69**, 1204–1214.
51. Winn,M.D., Ballard,C.C., Cowtan,K.D., Dodson,E.J., Emsley,P., Evans,P.R., Keegan,R.M., Krissinel,E.B., Leslie,A.G., McCoy,A. *et al.* (2011) Overview of the CCP4 suite and current developments. *Acta Crystallogr. D. Biol. Crystallogr.*, **67**, 235–242.
52. Vagin,A. and Teplyakov,A. (2010) Molecular replacement with MOLREP. *Acta Crystallogr. D. Biol. Crystallogr.*, **66**, 22–25.
53. Emsley,P. and Cowtan,K. (2004) Coot: model-building tools for molecular graphics. *Acta Crystallogr. D. Biol. Crystallogr.*, **60**, 2126–2132.
54. Murshudov,G.N., Vagin,A.A. and Dodson,E.J. (1997) Refinement of macromolecular structures by the maximum-likelihood method. *Acta Crystallogr. D. Biol. Crystallogr.*, **53**, 240–255.
55. Laskowski,R.A., MacArthur,M.W., Moss,D.S. and Thornton,J.M. (1993) PROCHECK: a program to check the stereochemical quality of protein structures. *J. Appl.Cryst.*, **26**, 283–291
56. McCoy,A.J., Grosse-Kunstleve,R.W., Adams,P.D., Winn,M.D., Storoni,L.C. and Read,R.J. (2007) Phaser crystallographic software. *J. Appl. Crystallogr.*, **40**, 658–674.
57. Adams,P.D., Grosse-Kunstleve,R.W., Hung,L.W., Ioerger,T.R., McCoy,A.J., Moriarty,N.W., Read,R.J., Sacchettini,J.C., Sauter,N.K. and Terwilliger,T.C. (2002) PHENIX: building new software for automated crystallographic structure determination. *Acta Crystallogr. D. Biol. Crystallogr.*, **58**, 1948–1954.
58. Romano,P., Gray,J., Horton,P. and Luan,S. (2005) Plant immunophilins: functional versatility beyond protein maturation. *New Phytol.*, **166**, 753–769.
59. Lucke,C. and Weiwad,M. (2011) Insights into immunophilin structure and function. *Curr. Med. Chem.*, **18**, 5333–5354.
60. Taneva,S.G., Munoz,I.G., Franco,G., Falces,J., Arregi,I., Muga,A., Montoya,G., Urbaneja,M.A. and Banuelos,S. (2008) Activation of

nucleoplasmin, an oligomeric histone chaperone, challenges its stability. *Biochemistry*, **47**, 13897–13906.
61. Akey,C.W. and Luger,K. (2003) Histone chaperones and nucleosome assembly. *Curr. Opin. Struct. Biol.*, **13**, 6–14.
62. Erickson,H.P. (2009) Size and shape of protein molecules at the nanometer level determined by sedimentation, gel filtration, and electron microscopy. *Biol. Proc. Online*, **11**, 32–51.
63. Cameron,D.L., Jakus,J., Pauleta,S.R., Pettigrew,G.W. and Cooper,A. (2010) Pressure perturbation calorimetry and the thermodynamics of noncovalent interactions in water: comparison of protein-protein, protein-ligand, and cyclodextrin-adamantane complexes. *J. Phys. Chem. B*, **114**, 16228–16235.
64. Cooper,A. (1999) Thermodynamic analysis of biomolecular interactions. *Curr. Opin. Chem. Biol.*, **3**, 557–563.
65. Bouchemal,K. and Mazzaferro,S. (2012) How to conduct and interpret ITC experiments accurately for cyclodextrin-guest interactions. *Drug Discov. Today*, **17**, 623–629.
66. Mattiroli,F., Gu,Y., Yadav,T., Balsbaugh,J.L., Harris,M.R., Findlay,E.S., Liu,Y., Radebaugh,C.A., Stargell,L.A., Ahn,N.G. *et al.* (2017) DNA-mediated association of two histone-bound complexes of yeast Chromatin Assembly Factor-1 (CAF-1) drives tetrasome assembly in the wake of DNA replication. *Elife*, **6**, e22799.
67. Chen,H., Li,B. and Workman,J.L. (1994) A histone-binding protein, nucleoplasmin, stimulates transcription factor binding to nucleosomes and factor-induced nucleosome disassembly. *EMBO J.*, **13**, 380–390.
68. Laskey,R.A., Mills,A.D., Philpott,A., Leno,G.H., Dilworth,S.M. and Dingwall,C. (1993) The role of nucleoplasmin in chromatin assembly and disassembly. *Philos. Trans. R. Soc. Lond. B Biol. Sci.*, **339**, 263–269.
69. Ramos,I., Fernández-Rivero,N., Arranz,R., Aloria,K., Finn,R., Arizmendi,J.M., Ausió,J., Valpuesta,J.M., Muga,A. and Prado,A. (2014) The intrinsically disordered distal face of nucleoplasmin recognizes distinct oligomerization states of histones. *Nucleic Acids Res.*, **42**, 1311–1325.
70. Ramos,I., Martin-Benito,J., Finn,R., Bretana,L., Aloria,K., Arizmendi,J.M., Ausio,J., Muga,A., Valpuesta,J.M. and Prado,A. (2010) Nucleoplasmin binds histone H2A-H2B dimers through its distal face. *J. Biol. Chem.*, **285**, 33771–33778.
71. Franco,A., Arranz,R., Fernandez-Rivero,N., Velazquez-Campoy,A., Martin-Benito,J., Segura,J., Prado,A., Valpuesta,J.M. and Muga,A. (2019) Structural insights into the ability of nucleoplasmin to assemble and chaperone histone octamers for DNA deposition. *Sci. Rep.*, **9**, 9487.
72. Andrews,A.J., Chen,X., Zevin,A., Stargell,L.A. and Luger,K. (2010) The histone chaperone Nap1 promotes nucleosome assembly by eliminating nonnucleosomal histone DNA interactions. *Mol. Cell*, **37**, 834–842.
73. Okuwaki,M., Sumi,A., Hisaoka,M., Saotome-Nakamura,A., Akashi,S., Nishimura,Y. and Nagata,K. (2012) Function of homo- and hetero-oligomers of human nucleoplasmin/nucleophosmin family proteins NPM1, NPM2 and NPM3 during sperm chromatin remodeling. *Nucleic Acids Res.*, **40**, 4861–4878.
74. Diedrich,G., Spahn,C.M., Stelzl,U., Schafer,M.A., Wooten,T., Bochkariov,D.E., Cooperman,B.S., Traut,R.R. and Nierhaus,K.H. (2000) Ribosomal protein L2 is involved in the association of the ribosomal subunits, tRNA binding to A and P sites and peptidyl transfer. *EMBO J.*, **19**, 5241–5250.
75. Lindstrom,M.S. and Zhang,Y. (2008) Ribosomal protein S9 is a novel B23/NPM-binding protein required for normal cell proliferation. *J. Biol. Chem.*, **283**, 15568–15576.
76. Xiao,H., Jackson,V. and Lei,M. (2006) The FK506-binding protein, Fpr4, is an acidic histone chaperone. *FEBS Lett.*, **580**, 4357–4364.
77. Dosztanyi,Z., Csizmok,V., Tompa,P. and Simon,I. (2005) The pairwise energy content estimated from amino acid composition discriminates between folded and intrinsically unstructured proteins. *J. Mol. Biol.*, **347**, 827–839.
78. Romero, Obradovic and Dunker,K. (1997) Sequence data analysis for long disordered regions prediction in the Calcineurin family. *Genome Inform. Ser. Workshop Genome Inform.*, **8**, 110–124.